ORNL/TM-2003/206

August 30, 2003

Prepared by: Gary E. Giles

Wood Pulp Digester Wall Corrosion Investigation

ORNL/TM-2003/206

WOOD PULP DIGESTER WALL CORROSION INVESTIGATION

Gary E. Giles

Date Published: August 2003

Prepared by
OAK RIDGE NATIONAL LABORATORY
Oak Ridge, Tennessee 37831-6415
managed by
UT-BATTELLE, LLC
for the
U.S. DEPARTMENT OF ENERGY
under contract DE-AC05-00OR22725

CONTENTS

LIST OF FIGURES

ACKNOWLEDGEMENTS

This work would not have progressed as well without the consultations of Professor Martha Salcudean and Dr. Eric Bibeau of Process Simulations, Ltd (PSL). The NWM code requires the existence of the PSL digester performance code, which they and others are developing.

Dr. James Park was responsible, with Professor Salcudean, for the original concept of using the lubrication theory to develop a code that would interface with the PSL code and provide detailed information in the layer near the wall. He was also responsible for the original mathematic development on which the NWM code is based and for suggesting a form of differencing that performed well on nonuniform meshes.

I would also like to thank Dr. Steve Pawel for his leadership of this project. His greater understanding of the field has prevented me from many a mistake or misstatement.

ABSTRACT

The modeling of the flow in a wood pulp digester is but one component of the investigation of the corrosion of digesters. This report describes the development of a Near-Wall-Model (NWM) that is intended to couple with a CFD model that determines the flow, heat, and chemical species transport and reaction within the bulk flow of a digester. Lubrication theory approximations were chosen from which to develop a model that could determine the flow conditions within a thin layer near the vessel wall using information from the interior conditions provided by a CFD calculation of the complete digester. The other conditions will be determined by coupled solutions of the wood chip, heat, and chemical species transport and chemical reactions. The NWM was to couple with a digester performance code in an iterative fashion to provide more detailed information about the conditions within the NW region. Process Simulations, Ltd (PSL) is developing the digester performance code. This more detailed (and perhaps more accurate) information from the NWM was to provide an estimate of the conditions that could aggravate the corrosion at the wall. It is intended that this combined tool [NWM-PSL) could be used to understand conditions at/near the wall in order to develop methods to reduce the corrosion.

However, development and testing of the NWM flow model took longer than anticipated and the other developments (energy and species transport, chemical reactions and linking with the PSL code) were not completed. The development and testing of the NWM are described in this report.

In addition, the investigation of the potential effects of a clear layer (layer reduced in concentration of wood chips) near the wall is reported in Appendix D. The existence of a clear layer was found to enhance the flow near the wall.

1. INTRODUCTION

Wood pulp digesters are tall (55–70 m) metal cylinder-like tanks used to treat wood chips with aggressive chemicals to make paper pulp. Digesters may have diameter changes along the height and may look more like a bottle with a wider section near the bottom. Schematic drawings of the exterior of the two digesters are shown in Fig. 1. The project funding this work was primarily interested in these two digesters. The Kamloops digester, located in Kamloops, BC, Canada, is 52 m tall and has a maximum diameter of 7.62 m. (The other digester shown is located in Spring Grove, Pennsylvania.) A heated mixture of wood chips and liquor is introduced near the top of the digester. The liquor is an aqueous solution of chemicals for breaking down the lignin (delignification). Delignification is accomplished by heating and intimately mixing the contents to accelerate penetration of the chemicals into the chips and to accelerate the desired chemical reactions. Lignin holds the cellulose fibers together and delignification frees the fibers so that they can be used to make paper. At several locations along the vertical side of the digester, liquor is extracted through a set of cylindrical screens, processed (generally heated or chemically modified), and reintroduced into the general digester flow from the central pipe called a down comer (not shown in Fig. 1). Several reintroduction regions at different levels are used to control delignification. The processed wood chips are extracted as pulp near the bottom of the digester. The wood chips hold their form without significantly changing size until they are extracted from the exit. Although the chips retain their form while in the digester, they become less dense and firm. The ejection of the wood chips actually separates the fibers into the desired wood pulp. In some digesters there is also a paddle-type rotating rake-arm near the bottom.

The conditions within the digester (high temperatures, process chemicals, wood extractives, potentially erosive flows, abrasion by the wood chips, etc.) will produce corrosion of the carbon steel walls (a common material for digesters). Initially, the walls are generally 0.05 m (2 in.) or more thick. Thinning by excessive corrosion can reduce pressure allowed in the digester, which can reduce the productivity. The working life of a digester is 20 or more years. Refurbishment costs to restore the productivity and lost production income during the maintenance can be prohibitive.

Local areas of excessive corrosion have been found in many digesters. However, this corrosion has not been identified with any specific flow pattern, chemical, or fluid condition. Although wood pulp digesters have been in use for many years, there is not a complete understanding of the fluid flow within the digester or of the conditions near the wall. Ad-hoc modifications to the general digester flows have been made over the years to modify the product or increase the efficiency of the process without a complete understanding of the conditions within the digester.

The goal of this project is to develop a better understanding of the conditions (chemical, fluid, and thermal) near the wall in a wood pulp digester, and thus predict and/or prevent conditions that would produce excessive corrosion.

The research path that was chosen for this project was to develop a set of equations describing the flow near the wall of the digester and incorporate the finite difference representation of these equations into a general digester performance code[1] being developed by Professor Salcudean and others of Process Simulations Ltd. (PSL). Thus, this project needed a set of easily solved equations that incorporate the physics of the fluid layer near the wall and which could exchange information with a code that simulates the interior flow. As explained in Sect. 3, a development of such a model based on the lubrication theory[2] was chosen. This set of equations was developed (Appendix A), implemented into the Near-Wall-Model (NWM) code (Appendix B), and tested by comparison to two different digester models and solution techniques (reported in Sect. 4). This direction was facilitated by PSL's prior involvement with the project and the digester industry. Also, many discussions with Professor Saludean, Dr. Bibeau, and others from PSL helped greatly in gaining some understanding of digesters and their physics.

A method of testing for the NWM code was devised that did not require complete coupling with the PSL digester code. A computational fluid dynamics (CFD) code (CFX4)[3] was used to estimate the fluid conditions within a simplified digester design. [CFX4 is a general finite volume CFD code that includes

models that are appropriate to the digester analysis (energy and species transport, chemical reactions). Although CFX4 has several solid/liquid flow models the applicability of these models to digester flow is not known. The initial stage of testing used only the fluid dynamics models of CFX4.]

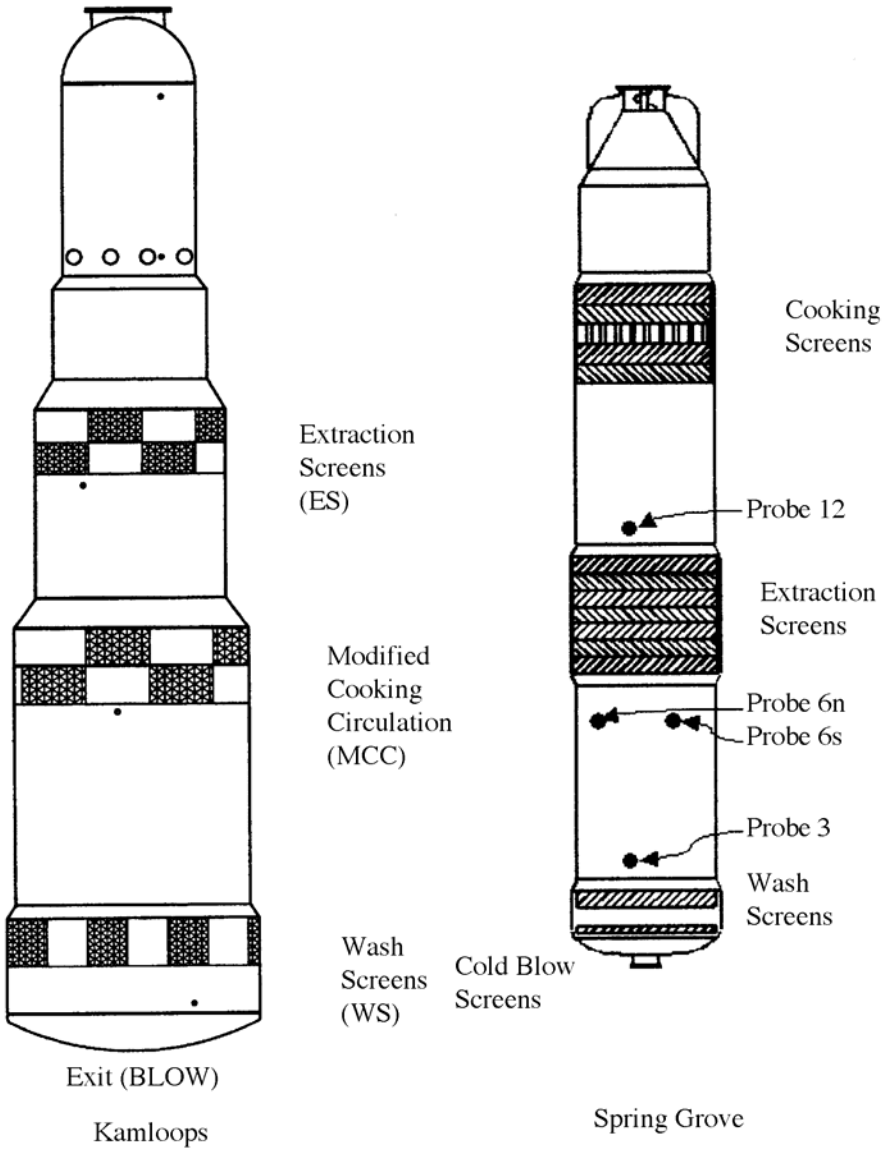

Fig. 1. Schematic drawings of two Kraft digesters.

A fine grid near the wall in the CFX4 model provided the conditions at the inner radial surface of the near wall (NW) layer from this complete interior flow model to the NWM code. The NWM produced an estimate of the pressure in the NW layer from these boundary conditions. If NWM emulates the flow physics correctly, then the NWM pressure estimate would agree with the pressure estimate produced by CFX4. In this one-way testing procedure, the information interpolated from the complete digester model is used to drive the solution in the NWM code. It is planned to extend into a full two-way communications in the next stage of the development. The two-way method would allow the interior

results to affect the NWM, and the NWM results would in turn affect the interior solution. This would produce detail information within the NW layer without having to finely discretize this region, thus providing less expensive but accurate solutions. However, the development and testing of the NWM in a one-way manner using CFX4 or the PSL code consumed the budget and time allowed for this project. Further development of the NWM to allow coupling with the PSL code awaits further funding.

The following sections and appendices summarize the development, implementation, and testing efforts of this project up to this time. Conclusions about the applicability of this approach are reported in Sect. 4.

2. LITERATURE SURVEY OBJECTIVES

A targeted literature search was made with specific objectives. This search did not represent a comprehensive exploration of prior art, but only an attempt to determine answers to specific questions. The first question was whether there were prior applications of approximate solutions to the flow near the wall of large process vessels. None were found that were applicable to digesters in the available literature. The second objective was to determine whether there were applications of a full CFD/Thermal/Chemical analysis of a digester. Although there were studies other than PSL's of a digester or digester-type devices, none of these were as complete as the PSL code nor offered additional insight that was helpful in this project.

The other goals of the literature search were: (1) determine the state of the art in liquid-solid flows and to see if this art could be helpful in this investigation; (2) determine if the literature on packed beds might be helpful; and (3) identify other corrosion theories (such as erosion-corrosion) that might explain the patterns of corrosion found in local areas of some digesters.

Only limited information was found that was helpful. In particular the PSL report draft and references within it (primarily the Harkonen[4] paper) were found that were useful to this investigation.

The details of the search for the liquid-solid flow information, packed beds, and the alternative corrosion theories are reported in Appendix C.

3. NWM DEVELOPMENT

This section (along with Appendix A) is an edited version of a document written by James E. Park, entitled "Boundary Conditions For The PSL Digester Model."[5] Park's document describes an approach to modeling the fluid near a digester wall using a development from the lubrication theory. The lubrication theory approach has been applied successfully to modeling flow in thin gaps between solid surfaces and even between a porous medium and a solid surface. The theory is applicable in thin regions next to solid boundaries where the viscous forces predominate over inertia forces. This approach was chosen for this project since the thin layer next to the wall should satisfy the limiting requirements, the type of solution would not require prior information about the flow direction, and the solution method for this analytical approach is very efficient.

The resulting code (NWM details in Appendix B) implements the most simple of the model family described in Appendix A. The discussion in this section and in Appendix A was edited to correct some minor errors, remove duplication, and to make the extracted notes consistent with the rest of this document.

3.1 DESCRIPTION

The solid boundaries of the digester (especially the vertical boundaries, the sides of the center pipe and vessel) influence the liquor/chip flow by preventing the liquor from leaving (zero normal velocity) and by bringing the tangential velocities to zero at the wall (normal assumption for solid walls in fluid

flow). The liquor/chip flow is hindered on the boundaries by dragging along the wall (friction) and flowing around the solid boundaries (momentum loss). Additionally, energy will be exchanged with the digester wall. Finally, various chemical exchanges between the liquor, the wood chips, and the wall may occur.

The aim of this discussion is to establish simplified models that replace the necessity of resolving (with a very fine mesh) the influence of the solid boundary on the flow within the digester. The scheme developed here is along the guidelines suggested by Professor Salcudean. The boundary conditions for the interior flow (volume of digester flow excluding the NW region) are calculated from interior information and a model of what is happening in the near wall region. The models described in this report are specific examples of the "smooth functions" suggested by Salcudean. It differs from her suggestions in that the boundary region is only one computational cell (of the interior region model) in height. For this development, the computational cell is usually 2 mm (less than the average wood chip width of 5 mm).

This section will describe a method of modeling boundary conditions for the fluid momentum equation in the PSL paper "Modeling of Kraft Two-Phase Digester Pulping Processes"[1] distributed at the task force meeting in Seattle in September of 1999 and in the PowerPoint slides[6] used in the PSL presentation at that same meeting. The details of the PSL equations and the numerical derivation of the Poisson Equation for pressure in the NW layer are contained in Appendix A.

The effect of the solid material in this simplified multiphase flow model (NWM) is accounted for by the momentum exchange in the liquid momentum equation only. By not including an additional solid momentum equation, the chip mass in the near wall region is assumed to retain the same momentum, energy, and chemical characteristics as the solid material at the top of this region. This approximation does not assume that a clear layer is maintained next to the wall, only that the changes in momentum and fraction of the solid particles are the same as in the layer of the interior solution next to the near-wall layer. It was intended that more accurate models for the solid momentum equation and boundary conditions for this equation, energy transfer, and chemistry change be developed during next stage. Adding the energy and species transports (advection-diffusion equations) should be straightforward. The complex chemical processes will be modeled in the same manner as the PSL code.

3.2 TYPES OF BOUNDARY FLOW

At least five types of boundary layer flow occur at various locations in a digester. One is the "classic" boundary layer, in which pressure, advection, and diffusion forces are balanced. The second is the lubrication layer, in which only the pressure and viscous forces are important. Normally, lubrication layers are modeled as flowing between two solid bounding surfaces. Both solids may be stationary and one may be porous (like the chip mass) or moving or both. These first two flow conditions occur over large portions of the digester wall/surface (except near inlets, outlets, and diameter changes). The third type is the impingement of a jet flow onto a solid boundary and occurs on surfaces opposite inlet streams from the center pipe (downcomer). The fourth is a separating boundary layer that occurs at step function diameter changes inside the vessel (associated with the physical boundaries of the screen ports). The fifth type is where an exit or inlet exists at the wall. This type occurs at screens, at downcomer outlets, and at the pulp outlet at the bottom of the vessel. Figure 2 shows typical flow for these boundary layers.

The fifth type of condition (entering or exiting of a jet from a wall can also cause the flow to separate (form recirculation regions where the flow is not necessarily parallel to the wall). In Fig. 2(e) the directions of the flow adjacent to the inlet/exit are highly dependent on the main flow in the digester and the flow rate in the inlet/exit. The flows along the wall may continue to progress in the same direction passing the inlet/exit, or they may reverse direction (converge on the inlet/outlet) as in the upper portion of that figure. This flow reversal can occur at either inlets or outlets.

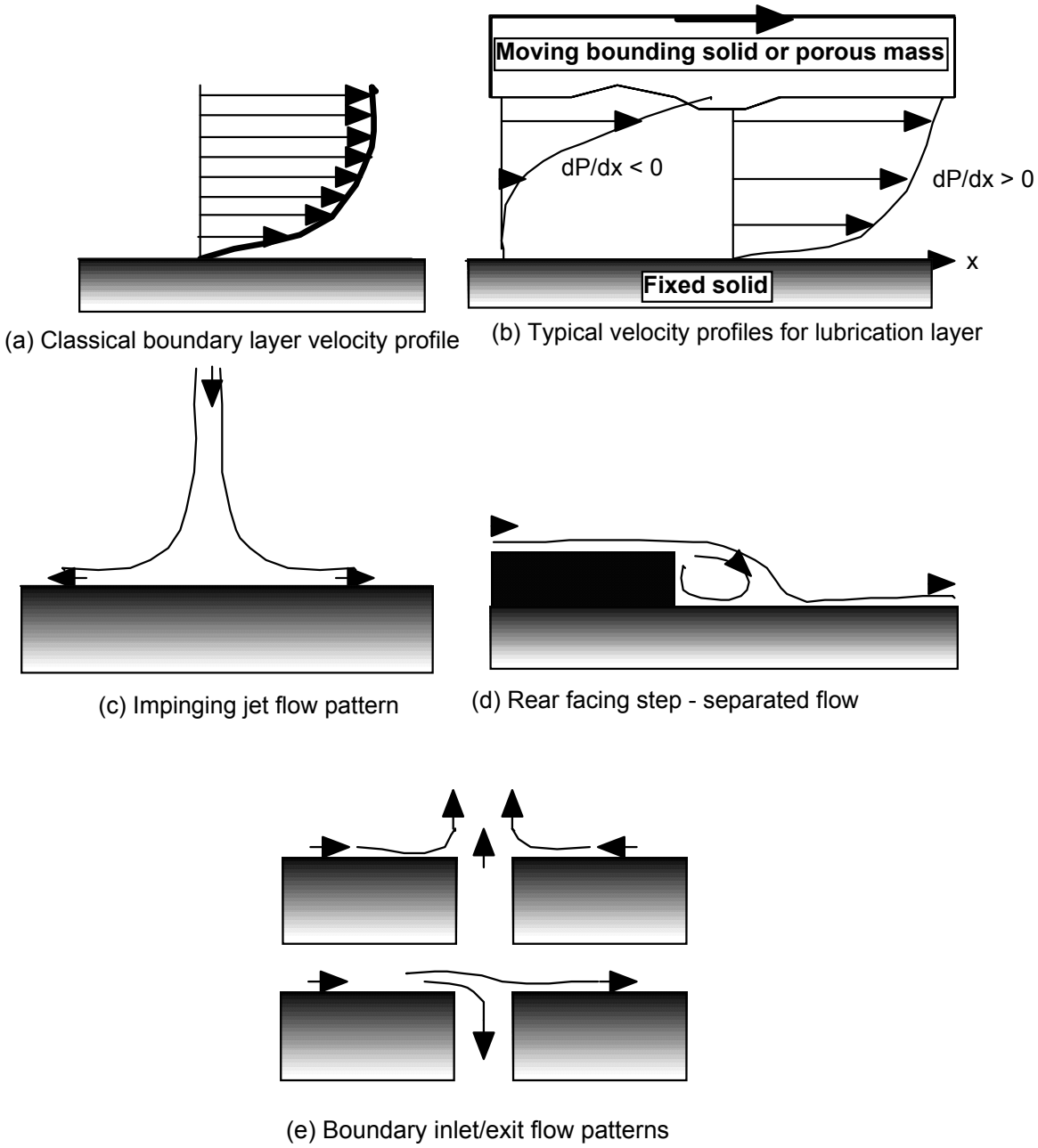

Fig. 2. Flow patterns and velocities for typical types of flow found in digesters.

Advection effects (the change in temperature or other physical properties by the movement of the fluid) may or may not be important in the boundary layer along the digester wall. If they are important, then this implies a preferred flow direction. In a digester, it is easy to imagine many different preferred flow directions on different portions of the wall. For example, the discharge from a nozzle impacts the outer wall and initiates boundary layers in all directions from the stagnation point [Fig. 2(c)]. With several nozzles in operation, these boundary flows will collide at some point, producing separation zones where the flow is redirected into the bulk volume. The calculation of these flows by constructing boundary layer solutions for a complete digester is at best impractical. (Boundary layer solutions require prior knowledge of the flow direction and distance from the start of the boundary layer. This information

changes with conditions and is difficult to obtain for a typical digester flow.) Likewise, numerical resolution of the boundary layers, using the full set of governing equations, is an economical impossibility. Finally, a balance between pressure and viscous effects may form between the digester wall and the flat sides of chips nearest to the wall. Basically, one type of flow (lubrication) is assumed to exist on the entire vertical wall of the digester. This assumption is an approximation and the accuracy of it must be tested.

What is needed is a formulation that will sense changes in flow direction, a formulation that captures impingement of jets, separation, etc. without additional assumptions being made about flow direction during the development. In other words, a formulation is needed that minimizes the directional bias that the advection terms introduce. A pressure-based formulation emerges from the lubrication assumptions for fluid flow. The assumptions that lead to the lubrication equations will apply only in a portion of the digester boundary layers, so development will include the advection terms but in a subordinate role. Details of the numerical derivation are contained in Appendix A. The implementation of this derivation is described in Appendix B.

To reiterate, Appendices A and B describe the development of a model and code that simulates the fluid flow conditions in a thin (approximately 2–5 mm) layer near the wall of the digester given the conditions at the top (or inner radius) of this near wall region. These conditions are given by a flow solution of more complete equations for solid/fluid flow in the interior of the digester. The next section describes the testing of the code and the conclusions that were drawn.

4. TESTING OF THE NEAR-WALL-MODEL (NWM) CODE

The initial stages of testing used a simple cylindrical volume (uniform radius) with very simple flow patterns, such as plug flow or swirling flow (adding a constant circumferential velocity) in turn or in combination if possible. In these cases, it was assumed that the liquid and solid flows have the same uniform axial velocity. Although these mathematically simple flow patterns might not be physically realistic for digesters, they allowed a step-by-step verification that the NWM mathematics.

4.1 SIMPLIFIED DIGESTER CFX RESULTS

To perform testing of more physically realistic situations, a two-dimensional axisymmetric model of a simplified digester was developed for CFX4 and CFX5. CFX4 is a general finite volume CFD code that uses a structured grid and includes many of the models that would be appropriate for a digester analysis. CFX5 is a more modern, unstructured mesh, general CFD code that has many of the same models as CFX4 with additional newer models particularly for solid/liquid flow and with more efficient numerical techniques. CFX5 was used in this project only for a few models, both as a check on the validity of CFX4 and to investigate the newer physical models unavailable in CFX4. All of the results reported here were performed on CFX4.

The geometrically simple model used in CFX4 was a right circular cylinder, Fig. 3. This model fits well within the geometric limitations of a structured mesh code like CFX4. The cylinder contains a fluid flowing within a nonmoving porous medium. The porous medium is not modeled explicitly but only by its effects on the fluid. The solid walls are included in the model only as boundary conditions (no-slip, no-flow boundaries). This simplified geometry offers some of the complexity of flow found in a typical digester. A central cylindrical region was removed from the fluid region to simulate a down-comer with a radius of 0.23 m and a length of 17.7 m from the top. This model had two inlets and two outlets. The main flow (FEED) entered at the top of the cylinder as a uniform plug flow (axial velocity = nonzero, radial velocity = zero). The other inlet (WD) was on the radial surface at the bottom of the down-comer. This inlet provided fluid with a radial outward velocity (axial velocity = zero). There was an outlet (ES) on the outer radius of the cylinder. (As suggested in the CFX4 manual, to avoid potential numerical difficulties, this outlet was modeled as an annular region extending outward for 1.0 m. See Fig. 3. at ES.)

A specified pressure was applied as a boundary condition on the outer radial surface of this extended outlet. The second outlet (BLOW) was located at the bottom of a smaller cylinder (radius = 0.23 m) that extends 1.0 m below the main cylindrical volume. A specified pressure boundary condition was applied on this surface. Both specified pressure boundary conditions were 0.0 Pa. The pressure used in the calculations does not have the hydrostatic pressure included. Hydrostatic pressure is the pressure produced by the weight of the fluid above a point. This simplification is made (in the NWM and CFX codes as well as the PSL digester code) to prevent the large numerical values of the pressure including the hydrostatic pressure from causing numerical difficulties when calculating a small pressure difference that may be important to the flow. Thus, the calculations can determine the sometimes very small pressure difference and thereby the driving force on the fluids between two points, without potentially introducing precision errors due to calculating a small difference between two large numbers. Thus, the boundary condition of 0.0 Pa represents the ambient pressure. In order to simplify the testing, the model was run in two dimensions. The porosity analyzed ranged from 1.0 (no solid fraction or porous medium) down to 0.1. The results shown here are all for a porosity of 0.3.

This model was analyzed by both the CFX4 and CFX5 CFD computer codes to produce estimates of the velocities, pressure, and temperatures near the wall of the model. Since this model was geometrically simple, it was possible to use a fine enough mesh to simulate the flow and allow the actual boundary layer thickness to be determined. (This level of refined mesh would not generally be possible in the full three-dimensional digester model.)

The volume was modeled as completely filled with a liquid. There are two inlets for this fluid. The top inlet (FEED) has a uniform axial velocity ranging from 1.744e-4 to 0.3488 m/s. On the centerline, the WD inlet has a uniform radial inlet velocity ranging from 4.9e-5 to 0.098 m/s. The relative strengths of the FEED and WD inlets were maintained for all cases. Since this made-up test case is only loosely based on an actual digester, the flow patterns and pressure gradient are not necessarily indicative of digester conditions.

The flow pattern produced in this simplified model exhibits some of the complex nature of the flow in a digester. For the inlet conditions modeled, generally the fluid at the top proceeds downward in a parallel manner with most of the feed inlet mass flow exiting the side vent. Thus, there is mostly axial flow above the ES outlet with more radial flow being established in the vicinity of this outlet. The majority of the FEED inlet flow exits the side vent at ES due to the relative strengths of the two inlets. Most of the WD inlet flow turns immediately downward and exits at BLOW. This flow pattern gives a fairly uniform steady flow down the side wall from the top to the side vent ES. Under this exit, there is upward flow along the wall into the ES exit. (The region below the exits in some digesters is often more aggressively corroded.[7] Reverse or upflow along the wall could exist in real digesters, and it might enhance the corrosion by transporting chemical species into unexpected regions.) Below 8.8 m, the flow is generally downward at the wall again with some recirculation and turning in the interior flow. The existence of parallel axial flow above the ES exit is consistent with the assumptions made in the development of the NWM code. The radial flow at ES and the reversing flow below ES are more problematic, however. The flow pattern in this simple digester model is highly dependent on the inlet and outlet conditions.

The flow patterns in real digesters are much more complex than the simplified patterns in this model. (See Sect. 4.3.) Thus, this model may provide a somewhat limited set of flow conditions to test against.

The mesh for the CFX4 2D model of this simplified digester was made fine enough near the wall to to resolve the boundary layer. Figure 4 shows the flow vectors for a position on the sidewall above the ES exit where the flow is parallel with the wall. The boundary layer is estimated to be 1.35 mm thick at this point. This estimate is based on the location of the flow vector that has the velocity of 99% of the bulk flow. Visually, this plot seems to show a thickness about 1 mm. However, the formal definition above produces the higher estimate. The boundary layer thickness varied from about 1 mm (near the top of the model) to almost 2mm (near the bottom) along the length of the digester wall. This estimate is also consistent with the results of comparison of the NWM code results with the CFX4 results. The best agreement in the pressure distribution, calculated by the NWM when compared with the CFX results, was

generally achieved using an assumed boundary layer thickness of 1–2 mm. The NWM requires that a constant NW layer thickness be assumed. As long as the assumed NW layer thickness is within the actual boundary layer, the approximation is correct. During the testing of the NWM, it was sometimes necessary to iterate on the assumed NW layer thickness in order to get a good match with the CFD code-produced pressure distribution. The automatic determination of the appropriate assumed NW layer thickness needs to be developed.

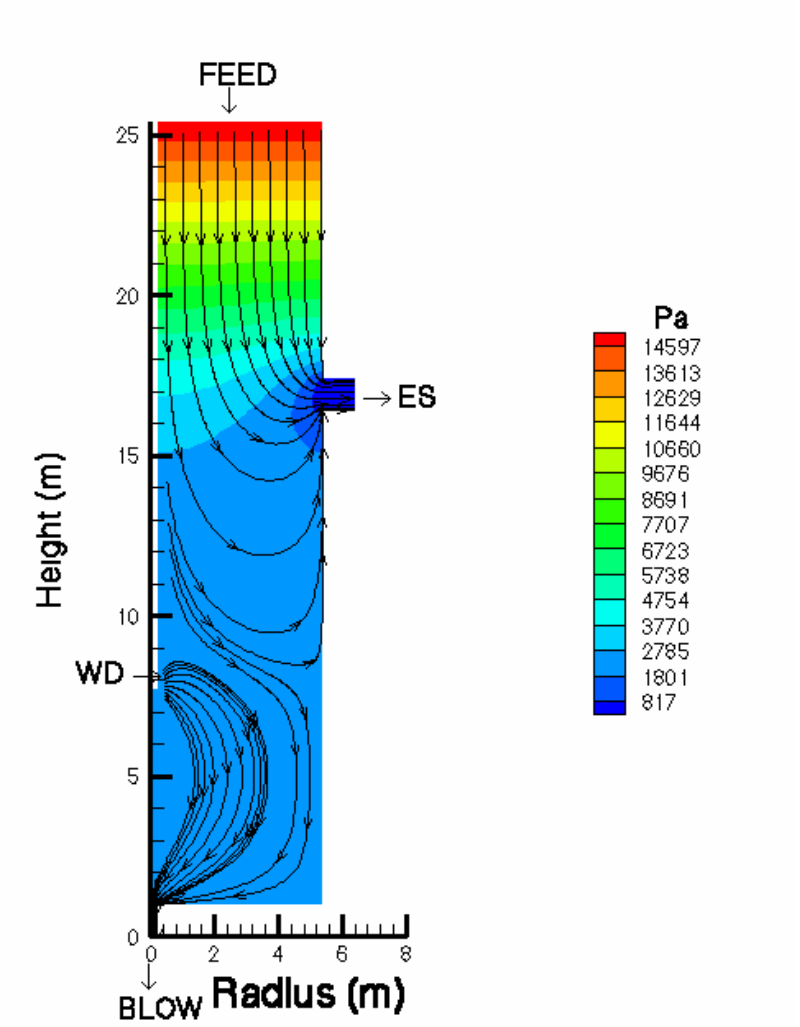

Fig 3. Two-dimensional model of a simplified digester. The axial coordinate for this mode is measured upward from the BLOW outlet. Inlet and outlets are marked. The calculated pressure is presented as color bands and selected streamlines show the major flow patterns. Laminar flow conditions with porosity of 0.3.

4.2 NWM RESULTS

The CFX4-produced flow variables were extracted along a surface representing the top of the assumed wall layer and used in one-way testing of the developed NWM code. For one-way testing, the information generated by CFX4 in a full model was used to drive the NWM calculations, and the information generated in the NWM code does not affect the interior solution. The CFX4 fluid calculations were performed in the whole volume (including the wall layer) assuming that normal CFD boundary conditions were used at the wall. Essentially, the NWM code takes velocity information from the

boundaries of the NW layer and calculates the pressure distribution. If the NWM code is correct, then the NWM pressure calculated should be nearly the same as was calculated in CFX4. This is a necessary, but not sufficient, condition for code correctness. However, such a match does not prove that the NWM code is correct in all conditions.

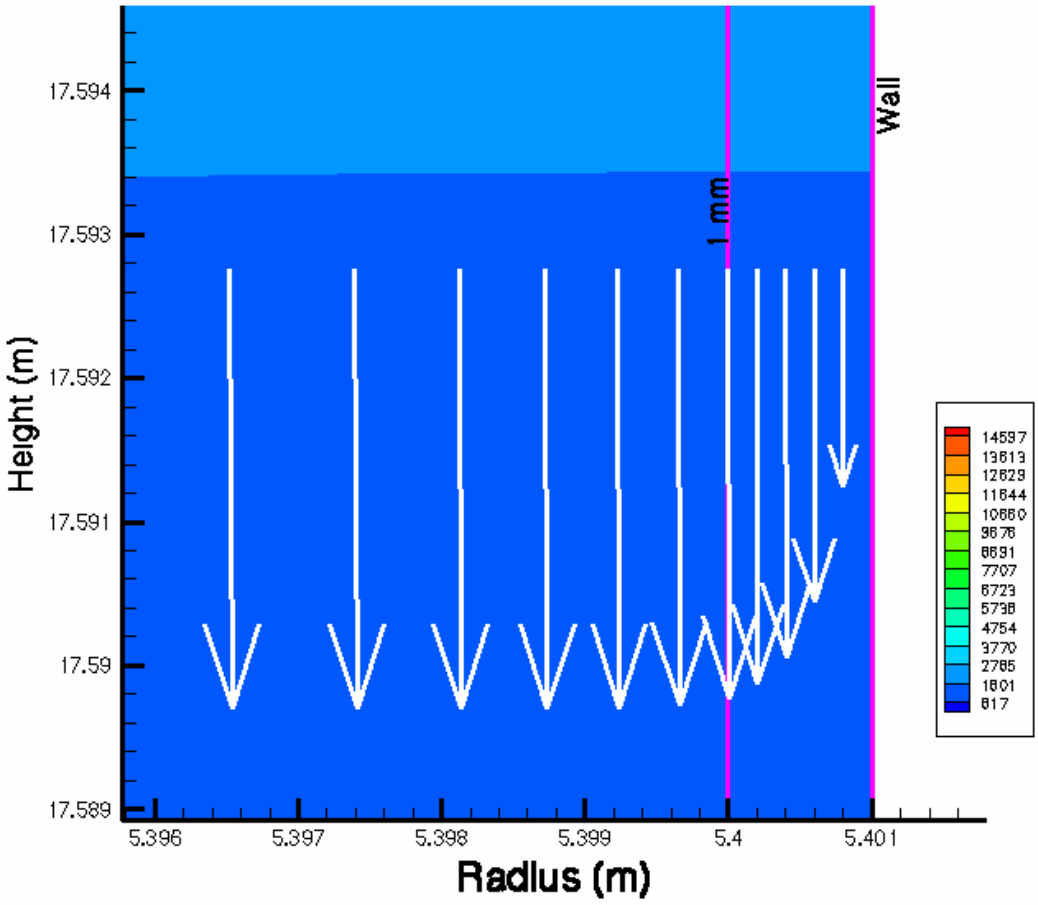

Fig. 4. Flow vectors in the boundary layer on the outer wall above the ES outlet with pressure (Pa) shown as color patterns.

Some of the early tests of the NWM were performed on uniform meshes. The CFX code requires the use of nonuniform meshes so the driving fluid parameters for the NWM (those calculated by CFX) were interpolated on a uniform mesh of 200 vertical locations. (For most of the models used in CFX, the number of axial nodes was 385.) Subsequently, a version of the NWM code was applied to see if this code could produce the same results as the CFX calculations on the same mesh. The NWM code calculates the local pressure in the NW layer by solving the Poisson equation. Since the NWM cannot calculate the flow correctly in the throat of the ES outlet due to the substantial pressure gradient arising from the radial flow across the near wall region, the pressure in this region is assumed to be the same as the CFX calculations. In fact, due to the flow turning into the exit, there is a nonnegligible pressure gradient across the assumed wall layer for a distance above and below the ES exit. For these reasons, the boundary of the Poisson equation solution was assumed to be applied a specified distance from the actual

edge of the outlet. This distance is determined by how well test runs match the CFX pressures and is a significant variable in the process of trying to get agreement between NWM and the CFX calculations.

The specified pressure boundary conditions at the top and bottom of the digester are reasoned from the fact that the flow must be turning in these regions, but must achieve a pressure balance with the main flow.

This case tested the one-way communication from the CFX code to the NWM code. If this test succeeded, then the more demanding two-way communication might be successful. [The two-way mode would have the CFX code model the interior flow while the NWM code produces estimates for the detailed wall flow. The shear stress estimated by NWM would be applied as boundary conditions on the CFD code and another iteration of the interior and then wall flows would be calculated. The solutions would be iterated until a steady solution is found (no change between iterations). The two-way mode would allow changes in the flow at the wall calculated by the NWM code to be communicated to the interior fluid calculations.]

The results of this test case provided some confidence that the basic approach and the implementation in the NWM code are correct. Figure 5 compares the calculated pressure with that produced by CFX4 for laminar conditions. The NWM results agree very well with the CFX results.

The Reduced Reynolds Number is much less than 1.0 in the wall layer. This is the upper limit of applicability of the lubrication theory.[2] The lubrication theory is expected to be accurate for Reduced Reynolds Number below 1.0. Thus, we expect the NWM that was developed from the lubrication theory assumptions to also be applicable in the digester problems.

Since the inlet flow conditions were arbitrarily picked for this calculation, several different conditions were modeled in CFX and compared to NWM results. Figure 6 shows the excellent match between the NWM and CFX4 pressure profiles for 5 different flow conditions. The flow multiplier indicated on the figure for each set of curves is applied to each boundary condition. For example, a flow multiplier of 1.0 has a velocity at the FEED of 8.72×10^{-2} m/s, while the velocity at WD is 2.45×10^{-2} m/s. For a flow multiplier of 2.0, the velocity at FEED is 1.744×10^{-1} m/s, and at WD it is 4.9×10^{-2} m/s or twice the 1.0 data). These calculations in NWM were performed for a nonuniform mesh that is the same as the axial discretization of the CFX calculations.

The encouraging performance of the NWM code on the nonuniform CFX4 mesh offered hope that the NWM would perform well when compared with the PSL-produced data for an actual digester model.

4.3 KAMLOOPS MODEL

Typical results from the PSL code were obtained for the Kamloops digester from Eric Bibeau of PSL. These results were preliminary since the PSL code is still under development. Sufficient information provided by PSL, together with some limited assumptions, made it possible to use the data in a similar manner as the CFX testing above.

4.3.1 PSL Results

Figure 7 presents the Kamloops digester model with inlet and outlet conditions as extracted from the data supplied by PSL. The top half of the digester model is shown in Fig. 7, while the bottom half is shown in Fig. 8. Figure 9 presents the pressure distribution in one case for the Kamloops digester. Streamlines are drawn on this figure to show the general nature of the flow induced by the 5 inlets and 6 outlets. This model is a two-dimensional axisymmetric case as were the PSL calculations. The results represent conditions calculated by the PSL code at a steady-state operation.

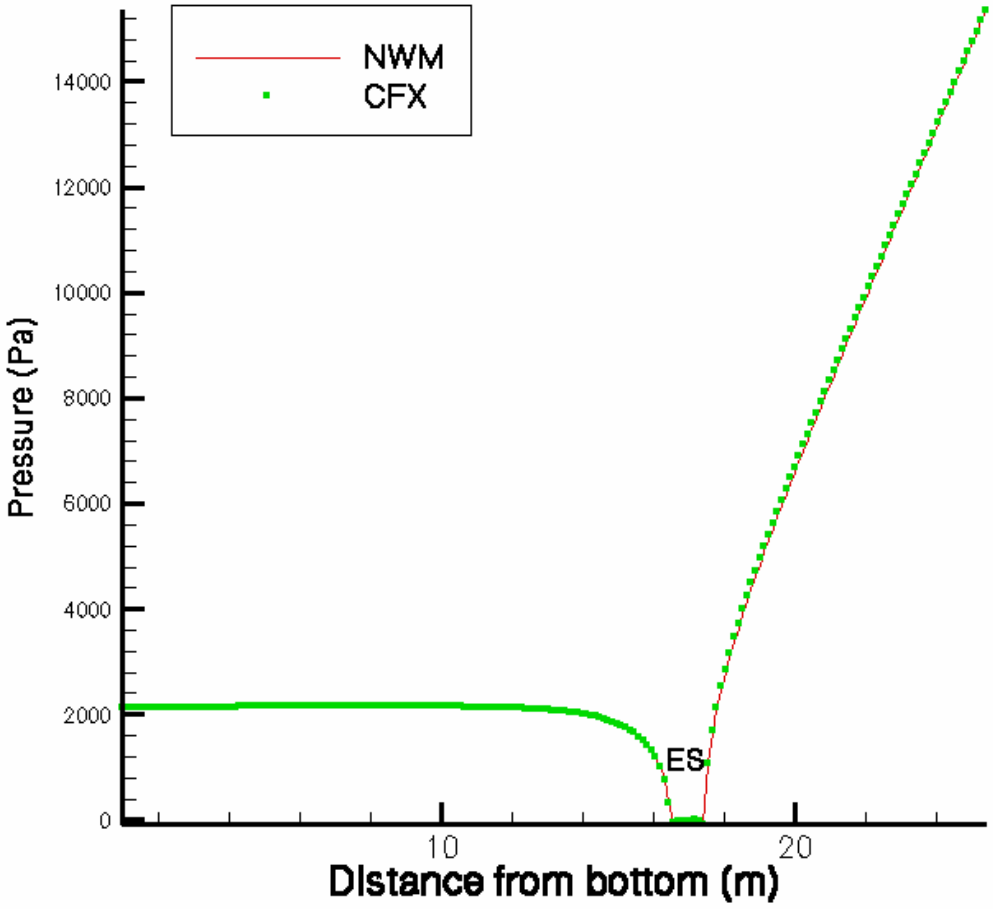

Fig. 5. Pressure distribution along the wall of the digester produced by NWM compared with the CFX results.

These results were taken from the PSL code while it was under development and more accurate results may be available later. However, for the purposes of determining if the NWM code could compute local pressure on a typical PSL code mesh, these results should be adequate. If the NWM code could produce results on such a mesh, then later more accurate data would be needed to confirm the adequacy of the NWM code as an adjunct to the PSL code.

Particularly, note the significant radial flow in the PSL data where the down-comer exits (inlets to the flow solution) are located. These flow sources also seem to generate substantial flow recirculation in the interior of the flow and on the outer radial wall flow impingements that might be classified as jets (or radial sheets in this two-dimensional model). The "jets" would produce a flow at the wall that is a challenge to the NWM technique. Although the possibility of these conditions was considered during the development, it was hoped that these were second order effects.

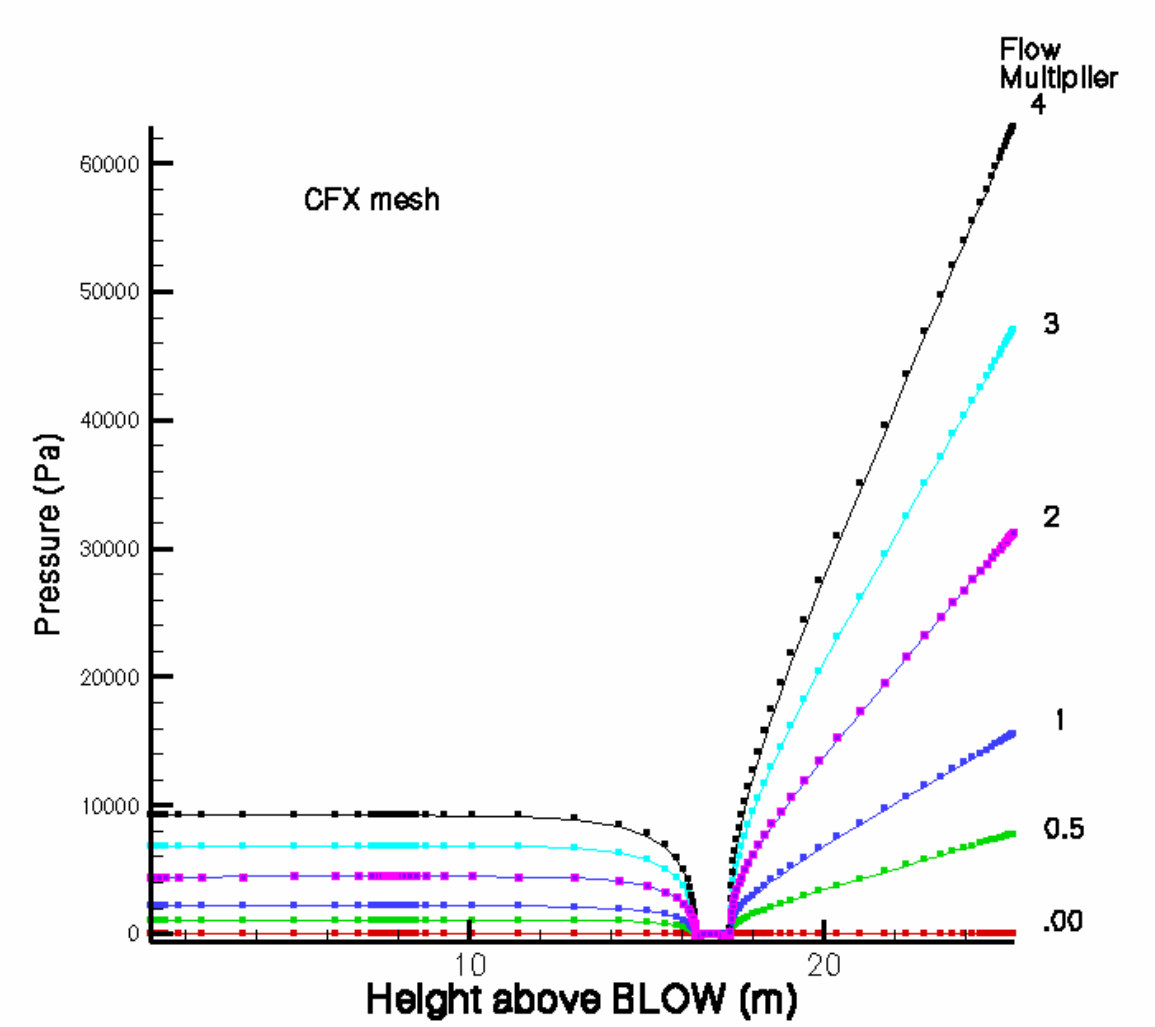

Fig. 6. Pressure distribution for different flow conditions (indicated by the multiplier) compared with CFX results. NWM results for a nonuniform mesh that is the same as the CFX mesh.

4.3.2 NWM Code Results

The excellent agreement with the PSL pressure distribution along the digester wall with the NWM results for the same mesh (nonuniform spacing, 98 nodes) is shown in Fig. 9. The gray rectangles represent the inlet or outlet regions on the sidewall of the digester where the pressure in the NWM calculations is assumed to be the same as the PSL data. The quality of the match is very encouraging for the future application of this technique in the two-way mode with the PSL code. These calculations assumed no advection as described in Appendix A. The nature of the comparison was not significantly modified by small variations in the assumed NW layer thickness.

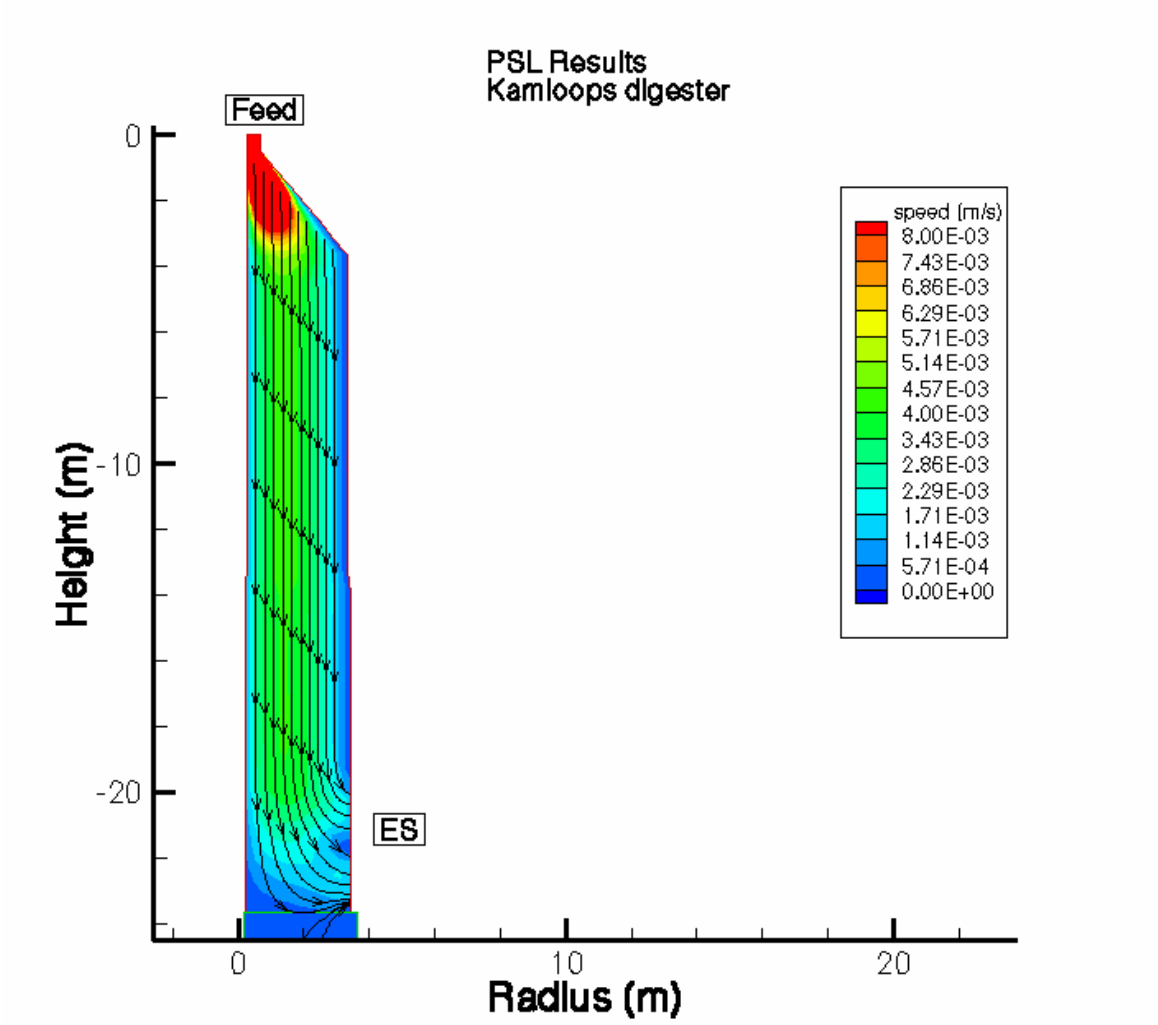

Fig. 7. Top half of the Kamloops digester model from the PSL data showing inlet and outlet locations. Flow speed contours and streamlines show the general flow pattern.

4.3.3 Conclusions

The development of the NWM model from the lubrication theory has been successful in producing a detailed model that**,** after adding the pertinent physics (heat and species transport and chemical reactions)**,** may be applicable to the PSL digester performance code**.** This combined set of models should be able to obtain detailed information about the near-wall conditions and interaction of flow, heat, and chemical species that contribute to corrosion.

This very important first step in the overall project goal (development of the NWM) has been successful.

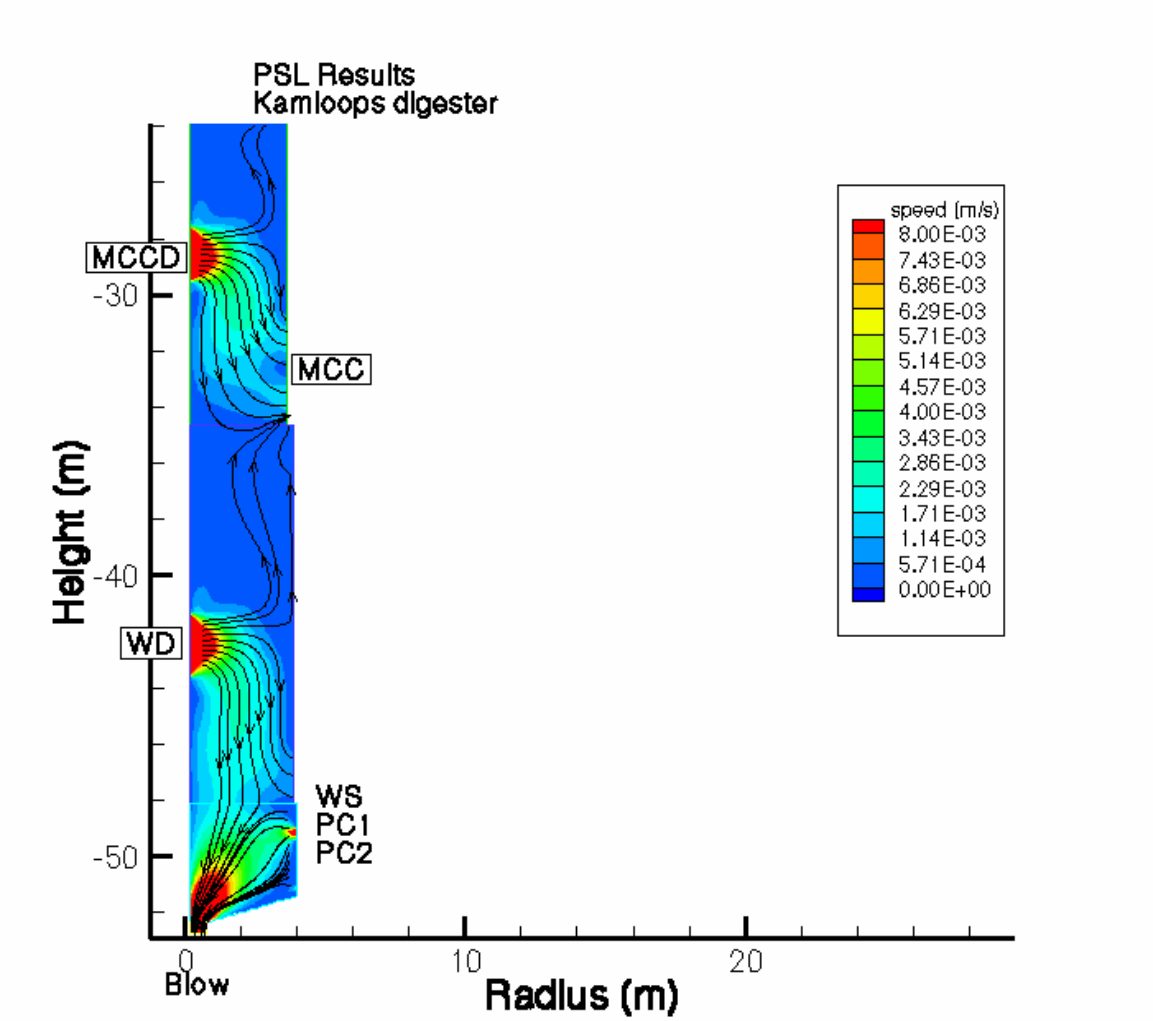

Fig. 8. Bottom half of the Kamloops digester model from the PSL data showing inlet and outlet locations. Flow speed contours and streamlines show more complex flow patterns.

As discussed in Appendix D, the possible existence of a clear layer might provide a faster transfer of chemical species (compared to the bulk flow) and thus, could significantly alter the corrosive conditions near the wall. These conditions may be very different from the bulk conditions, particularly above the topmost exit and in regions where up flow might be expected (below the exits).

4.3.4 Future Work

Although the development of the NWM was done in general cylindrical coordinates, all of the analyses reported were done for a two-dimensional model. The NWM will have to be tested against a three-dimensional model.

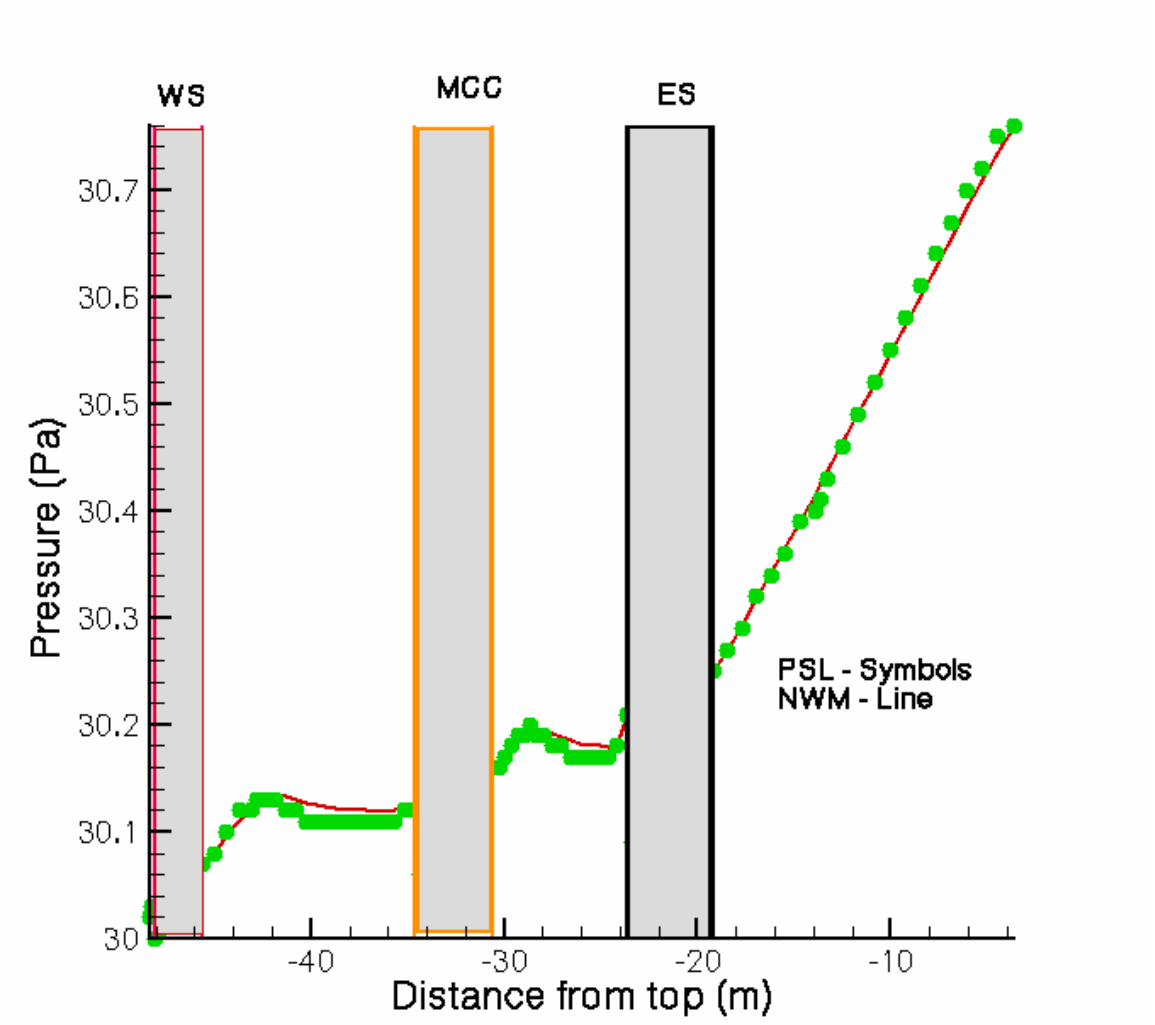

Fig. 9. Pressure distributions from the PSL data and the NWM code (nonoptimized) for a nonuniform mesh with a 2.0 mm assumed near wall layer thickness.

As stated before, the effective use of the NWM as a detailed model in the PSL code will require the addition of physical models for the heat transport, species transport, and chemical reactions that will control much about the conditions near the wall.

Heat transport will require the development of an energy equation that will couple the conductive and advective transport of heat. The advection of heat is the transport of heat by the flow and thus is dependent on the NWM results. The chemical reactions models will provide heat sources/sinks to the energy equation and source/sinks of species to the chemical transport model. The transport of chemical species (diffusion and advection) will control the rate of the chemical reactions, which are also dependent on the temperature. Thus, all of the equations are interrelated or coupled. The development of effective mathematical techniques to couple these equations with the PSL code could be challenging. In addition, the present version of NWM treats the solid momentum by the simplifying assumption that is the same as the bulk or interior solution and does not change across the NW layer. In reality the solid momentum equation (which describes the response of the wood chips to the local fluid velocity) will be different from this assumption. In the limited testing performed, this should not be a significant error as shown by

the excellent match in Sect. 4.3. However, in order to calculate an accurate set of conditions in the NW layer, this affect will have to be included.

At the conclusion of the development and successful coupling with the PSL digester code, the detailed information about the conditions (temperature, concentration, velocity) in the layer near the wall should allow estimates of localized instantaneous corrosion rates. Using the combined models, the modification of the corrosion by process and/or design changes should be possible.

REFERENCES

1. P. He, M. Salcudean, I. Gartshore, and E. L. Bibeau, "Modeling of Kraft Two-Phase Digester Pulping Process," Digester Wall Corrosion Task Force Meeting, Seattle, WA, September 7–8, 1999.
2. H. Schlichting, *Boundary Layer Theory*, 7th ed., McGraw-Hill, New York, 1979.
3. *CFX 4.4.1 Solver*, AEA Technology, PLC, Harwell, UK, 2002.
4. E. Harkonen, "A Mathematic Model For Two-Phase Flow In A Continuous Digester," *J. TAPPI*, 70, no. 12, pp.12–126,. December 1987.
5. J. E. Park, "Boundary Conditions For The PSL Digester Model," subcontractor report to G. E. Giles, March 16, 2001.
6. P. He, M. Salcudean, I. Gartshore, and E. L. Bibeau "Modeling of Kraft Two-Phase Digester Pulping Process," PowerPoint presentation, Digester Wall Corrosion Task Force Meeting, Seattle, WA, September 7–8, 1999.
7. S. J. Pawel, D. W. Townley, M. E. Gorog, D. F. Wilson, "Correlation of the Process Data and Electrochemical Noise to Assess Kraft Digester Corrosion: Kamloops Experiment," ORNL/TM-2002/33, April 2002.

APPENDIX A. NWM DEVELOPMENT

This appendix is an edited version of a document written by J. E. Park.[A1] Park's document describes an approach to modeling the fluid near a digester wall using a development from the lubrication theory. The discussion in this section was edited to correct some minor errors, remove duplication with, and to make these notes consistent with the rest of this document.

A.1 DESCRIPTION

The aim of this discussion is to establish simplified models that replace the necessity of resolving or ignoring the influence of the solid boundary on the flow within the digester.

This appendix will describe a method of modeling boundary conditions for Eq. (9) in the PSL paper "Modeling of Kraft Two-Phase Digester Pulping Processes"[A2] distributed at the Task Force meeting in Seattle, WA, in September of 1999 and in the Power Point slides[A3] used in the PSL presentation at that same meeting. The momentum equation is repeated here as Eq. (A.1.1) (written as in the PSL documents):

$$\frac{D\varepsilon_2\overline{\rho}_f\overline{V}_f}{Dt} = \overline{\mu}_f\nabla^2\varepsilon_2\overline{V}_f - \alpha_{ij}(\overline{V}_f - \overline{V}_s) - \varepsilon_2\nabla\overline{p}_f + \overline{V}_s m_{12} + \varepsilon_2\overline{\rho}_f\overline{F}_f \ , \qquad \text{(A.1.1)}$$

where

ε_2 = fraction of volume occupied by liquid,
ρ_f = fluid density,
V = velocity vector (subscript f = fluid, subscript s = solid) ,
μ_f = fluid viscosity,
α_{ij} =flow resistance tensor,
p_f = fluid pressure,
m_{12} = mass source from solid to liquid phases,
F_f = body force on the liquid,
t = time.

The overscore (which denotes averages) is omitted on all terms below. Note that the gravity terms are not included in the PSL equations.

Equation (11) from the same document (the mass conservation equation for the liquid) is also used and repeated here as Eq. (A.1.2.)

$$\nabla\cdot\varepsilon_2\rho_f V_f + \nabla\cdot\varepsilon_1\varepsilon_{12}\rho_f V_s - m_{12} = 0 \ , \qquad \text{(A.1.2)}$$

where

ε_1 = fraction of volume occupied by wood chips,
ε_{12} = fraction of chip volume occupied by liquid within chip.

Modeling required for the solid momentum boundaries, the energy transfer, and the chemistry will not be considered during this initial stage of the development. Adding the energy and species transports (advection-diffusion equations) should be straightforward.

In order to determine the conditions within the NW layer, a formulation that will sense changes in flow direction automatically is needed. In other words, a formulation that captures impingement of jets, separation, etc. automatically. That is, a formulation that minimizes the directional bias that the advection

terms introduce. A pressure-based formulation emerges from the lubrication assumptions for fluid flow. The assumptions that lead to the lubrication equations will apply only in a portion of the digester boundary layers, so development will include the advection terms but in a subordinate role.

A.2 DEVELOPMENT

The starting point for this development is the model for digester flow developed at PSL. To begin, note that the momentum equations given for the liquid flow in a digester have two different forms. Equation (9) in the PSL paper is less complex (repeated as Eq. (A.1.1) above). With the addition of the gravity term, this will be the starting point. Equation (11) in the same paper, the mass conservation equation for the liquid, will also be used and is repeated above as Eq. (A.1.2).

The PSL program works with the equations in a generalized curvilinear coordinate system using block-structuring techniques to fit the cell faces to the solid boundaries. This development will use the classic cylindrical coordinate system. The notation closely follows that used in the PSL paper, except that the overscores used to denote averages have been dropped and vectors are displayed with arrows above, e. g. $\vec{V}_f$ for the fluid velocity vector. Subscripts *f* and *s* indicate fluid and solid properties respectively. According to Professor Salcudean's notes, the symbol α_{ij} denotes a symmetric flow resistance tensor.

From the right-hand side of Eq. (A.1.1), the term for the momentum exchange between the chips and the liquid and the gravitation body force on the liquid (called "extra momentum" here) is defined as

$$EXMom = -\alpha_{ij}\left(\vec{V}_f - \vec{V}_s\right) + \vec{V}_s m_{12} + \varepsilon_2 \rho_f F_f \ , \qquad \text{(A.2.1)}$$

Note that the movement of the solid material in the wall layer is reflected in this first stage of the development by the terms in Eq. (A.2.1) containing the solid velocity ($\vec{V}_s$). The force on the liquid due to the drag of the wood chips is determined by the first term in Eq. (A.2.1). The momentum of the mass leaving (or entering) the wood chip is described by the second term. The solid velocity is taken from the interior solution and is not modified by the solution to the equations below. The solid momentum equation will be added later. For all test cases reported here, the mass source to/from the chip is assumed to be zero. For the first case used in Sect. 4 (flow through porous medium), there are no chips in the fluid. The porous medium represents the chip mass. Thus, the V_s and m_{12} terms are zero. For the second case (comparison with PSL data for the Kamloops digester), the zero m_{12} assumption is also used in the thin near wall region. This assumption was not made by PSL in the interior of the digester.

The components of the velocity vector are : $\vec{V}_f = u_f \vec{n}_r + v_f \vec{n}_\theta + w_f \vec{n}_z$.

The three components of the fluid momentum equation, Eq. (A.1.1), are:

$$\frac{\partial \varepsilon_f \rho_f u_f}{\partial t} + \frac{u_f}{r}\frac{\partial\left(r\varepsilon_2 \rho_f u_f\right)}{\partial r} + \frac{v_f}{r}\frac{\partial\left(\varepsilon_2 \rho_f u_f\right)}{\partial \theta} + w_f \frac{\partial\left(\varepsilon_2 \rho_f u_f\right)}{\partial z} - \frac{\varepsilon_2 \rho_f v_f^2}{r} + \varepsilon_2 \frac{\partial p}{\partial r} - \varepsilon_2 \rho_f g_r =$$
$$\mu_f \left[\frac{\partial}{\partial r}\left(\frac{1}{r}\frac{\partial\left(\varepsilon_2 r u_f\right)}{\partial r}\right) + \frac{1}{r^2}\frac{\partial^2 \varepsilon_2 u_f}{\partial \theta^2} - \frac{2}{r^2}\frac{\partial \varepsilon_2 v_f}{\partial \theta} + \frac{\partial^2 \varepsilon_2 u_f}{\partial z^2}\right] + \vec{n}_r \cdot EXMom \qquad \text{(A.2.2)}$$

$$\frac{\partial \varepsilon_f \rho_f v_f}{\partial t} + \frac{u_f}{r}\frac{\partial\left(r\varepsilon_2 \rho_f v_f\right)}{\partial r} + \frac{v_f}{r}\frac{\partial\left(\varepsilon_2 \rho_f v_f\right)}{\partial \theta} + w_f \frac{\partial\left(\varepsilon_2 \rho_f v_f\right)}{\partial z} - \frac{\varepsilon_2 \rho_f u_f v_f}{r} + \frac{\varepsilon_2}{r}\frac{\partial p}{\partial \theta} - \varepsilon_2 \rho_f g_\theta = \mu_f\left[\frac{\partial}{\partial r}\left(\frac{1}{r}\frac{\partial\left(\varepsilon_2 r v_f\right)}{\partial r}\right) + \frac{1}{r^2}\frac{\partial^2 \varepsilon v_f}{\partial \theta^2} - \frac{2}{r^2}\frac{\partial \varepsilon_2 u_f}{\partial \theta} + \frac{\partial^2 \varepsilon_2 v_f}{\partial z^2}\right] + \vec{n}_\theta \cdot EXMom \quad , \tag{A.2.3}$$

$$\frac{\partial \varepsilon_f \rho_f w_f}{\partial t} + \frac{u_f}{r}\frac{\partial\left(r\varepsilon_2 \rho_f w_f\right)}{\partial r} + \frac{v_f}{r}\frac{\partial\left(\varepsilon_2 \rho_f w_f\right)}{\partial \theta} + w_f \frac{\partial\left(\varepsilon_2 \rho_f w_f\right)}{\partial z} + \varepsilon_2 \frac{\partial p}{\partial z} - \varepsilon_2 \rho_f g_z = \mu_f\left[\frac{1}{r}\frac{\partial}{\partial r}\left(r\frac{\partial\left(\varepsilon_2 u_f\right)}{\partial r}\right) + \frac{1}{r^2}\frac{\partial^2 \varepsilon_2 w_f}{\partial \theta^2} + \frac{\partial^2 \varepsilon_2 w_f}{\partial z^2}\right] + \vec{n}_z \cdot EXMom \quad . \tag{A.2.4}$$

The gravity forces are included explicitly in this formulation instead of being included in the EXMom terms.

Under the assumptions used to derive the lubrication equations, or the conventional boundary layer equations, the radial pressure gradient is determined to dominate the radial momentum Eq. (A.2.2), and all but the radial viscous terms are determined to be negligible in both the angular and axial momentum equations. With those assumptions, defining

$$ANGex = \left[\frac{u_f}{r}\frac{\partial\left(r\varepsilon_2 \rho_f v_f\right)}{\partial r} + \frac{v_f}{r}\frac{\partial\left(\varepsilon_2 \rho_f v_f\right)}{\partial \theta} + w_f \frac{\partial\left(\varepsilon_2 \rho_f v_f\right)}{\partial z} + \frac{\varepsilon_2 \rho_f u_f v_f}{r}\right] + \varepsilon_2 \frac{1}{r}\frac{\partial p}{\partial \theta} - \vec{n}_\theta \cdot EXMom \quad , \tag{A.2.5}$$

Eq. (A.2.3) becomes

$$\mu_f\left[\frac{\partial}{\partial r}\frac{1}{r}\frac{\partial\left(r\varepsilon_2 v_f\right)}{\partial r}\right] \approx \mu_f\left[\frac{\partial}{\partial r}\frac{\partial\left(\varepsilon_2 v_f\right)}{\partial r}\right] \equiv ANGex \quad , \tag{A.2.6}$$

Similarly, Eq. (A.2.4) becomes

$$AXMex = \left[\frac{\partial \varepsilon_2 \rho_f w_f}{\partial t} + \frac{u_f}{r}\frac{\partial\left(\varepsilon_2 r \rho_f w_f\right)}{\partial r} + \frac{v_f}{r}\frac{\partial\left(\varepsilon_2 \rho_f w_f\right)}{\partial \theta} + w_f \frac{\partial\left(\varepsilon_2 \rho_f w_f\right)}{\partial z}\right] + \varepsilon_2 \frac{\partial p}{\partial z} - \varepsilon_2 \rho_f g_z - \vec{n}_z \bullet EXMom \quad , \tag{A.2.7}$$

and

$$\frac{\mu_f}{r}\frac{\partial}{\partial r}\left(r\frac{\partial \varepsilon_2 w_f}{\partial r}\right) \approx \mu_f \frac{\partial}{\partial r}\left(\frac{\partial \varepsilon_2 w_f}{\partial r}\right) \equiv AXMex \quad . \tag{A.2.8}$$

At this point the time derivatives have been dropped, thus making this development a steady state analysis. Further, it is assumed that either *ANGex* and *AXMex* are not functions of *r* in the boundary layers or they represent radial averages over the boundary layers. Also, the effect of boundary curvature has been removed by eliminating an *r* from Eqs. (A.2.6) and (A.2.8). This allows Eqs. (A.2.6) and (A.2.8) to be integrated over a thin region next to the boundary without dealing with computationally inefficient Bessel functions. [The large diameter of most digesters (on the order of 5 m) would make this approximation appropriate.] The result is

$$\varepsilon_2 v_f(r) = \frac{ANGex}{2\mu_f}\left[r^2 - r\left(r_o + r_i\right) + r_o r_i\right] + \frac{\left[\varepsilon_2 v_{fo} - \varepsilon_2 v_{fi}\right]}{r_o - r_i}\, r + \frac{\varepsilon_2 v_{fi} r_o - \varepsilon_2 v_{fo} r_i}{r_o - r_i}. \tag{A.2.9}$$

In these equations, v_{fi} and v_{fo} are the angular velocities, and w_{fi} and w_{fo} are the axial velocities at the mesh locations r_i and r_o, where r_i and r_o are the edge radii of the computational cells nearest to the boundary being treated.

$$\varepsilon_2 w_f(r) = \frac{AXMex}{2\mu_f}\left[r^2 - r\left(r_o + r_i\right) + r_o r_i\right] + \frac{\left[\varepsilon_2 w_{fo} - \varepsilon_2 w_{fi}\right]}{r_o - r_i}\, r + \frac{\varepsilon_2 w_{fi} r_o - \varepsilon_2 w_{fo} r_i}{r_o - r_i}. \tag{A.2.10}$$

The next step is to multiply the fluid continuity equation [Eq. (A.2.9)] by *rdr* and integrate across the boundary layer, from r_i to r_o:

$$\begin{aligned}\int_{r_i}^{r_o} \nabla \bullet \left(\varepsilon_2 \rho_f V_f\right) r dr &= \int_{r_i}^{r_o} \frac{1}{r}\frac{\partial\left(\varepsilon_2 r \rho_f u_f\right)}{\partial r} r dr + \int_{r_i}^{r_o} \frac{1}{r}\frac{\partial\left(\varepsilon_2 \rho_f v_f\right)}{\partial \theta} r dr + \int_{r_i}^{r_o} \frac{\partial\left(\varepsilon_2 \rho_f w_f\right)}{\partial z} r dr \\ &= \int_{r_i}^{r_o} \dot{m}_{12} r dr - \int_{r_i}^{r_o} \nabla \cdot \left(\varepsilon_2 \varepsilon_{11} \rho_f V_s\right) r dr\end{aligned}. \tag{A.2.11}$$

The first term in the center section of Eq. (A.2.11) is integrated by inspection. It directly applies the physical boundary condition and a value calculated in the interior using the full PSL model. Thus,

$$\int_{r_i}^{r_o} \frac{1}{r}\frac{\partial\left(\varepsilon_2 r \rho_f u_f\right)}{\partial r} r dr = \left(\varepsilon_2 r_o \rho_f u_f\right)\Big|_{r_o} - \left(\varepsilon_2 r_i \rho_f u_f\right)\Big|_{r_i}. \tag{A.2.12}$$

The second term in Eq. (A.2.11) is integrated using Eq. (A.2.9) for the angular velocity v_f and the third term is integrated using Eq. (A.2.10) for the axial velocity w_f.

$$\int_{r_i}^{r_o} \frac{1}{r}\frac{\partial\left(\varepsilon_2 \rho_f v_f\right)}{\partial \theta} r dr = \frac{\partial}{\partial \theta}\left[\rho_f\left[-\left(\frac{ANGex}{12\mu_f}\right)\left(r_o - r_i\right)^3 + \frac{1}{2}\left(\varepsilon_2 v_{fo} + \varepsilon_2 v_{fi}\right)\left(r_o - r_i\right)\right]\right]. \tag{A.2.13}$$

$$\int_{r_i}^{r_o} \frac{\partial\left(\varepsilon_2 \rho_f w_f\right)}{\partial z} r dr = \frac{\partial}{\partial z}\left[\rho_f\left[\begin{aligned}&-\left(\frac{AXMex}{24\mu_f}\right)\left(r_o^2 - r_i^2\right)\left(r_o - r_i\right)^2 \\ &+\frac{1}{6}\left(r_o - r_i\right)\left(\varepsilon_2 w_{fo}\left(2r_o + r_i\right) + \varepsilon_2 w_{fi}\left(r_o + 2r_i\right)\right)\end{aligned}\right]\right]. \tag{A.2.14}$$

The final steps in this development are to rearrange Eq. (A.2.11)–(A.2.14) to develop a Poisson equation for the liquid pressure field along the solid boundary.

$$\begin{aligned}
&\frac{(r_o - r_i)}{r}\frac{\partial}{\partial\theta}\left[\left(\frac{\rho_f \varepsilon_2}{12\mu_f}\right)\frac{\partial p}{\partial\theta}\right] + (r_o^2 - r_i^2)(r_o - r_i)^2\frac{\partial}{\partial z}\left[\left(\frac{\rho_f \varepsilon_2}{24\mu_f}\right)\frac{\partial p}{\partial z}\right] \\
&\qquad = -\left[(\varepsilon_2 r_o \rho_f u_f)\big|_{r_o} - (\varepsilon_2 r_i \rho_f u_f)\big|_{r_i}\right] \\
&\qquad - (r_o - r_i)^3\frac{\partial}{\partial\theta}\left[\left(\frac{\rho_f \varepsilon_2}{12\mu_f}\right)\left[ADV_\theta - \vec{n}_\theta \bullet EXMom\right]\right] \\
&\qquad + \frac{r_o - r_i}{2}\frac{\partial}{\partial\theta}\left[\rho_f(\varepsilon_2 v_{fo} + \varepsilon_2 v_{fi})\right] \\
&\qquad - (r_o^2 - r_i^2)(r_o - r_i)^2\frac{\partial}{\partial z}\left[\left(\frac{\rho_f}{24\mu_f}\right)\left[ADV_z - \vec{n}_z \bullet EXMom\right]\right] \\
&\qquad + \frac{(r_o - r_i)}{6}\frac{\partial}{\partial z}\left[\rho_f(\varepsilon_2 w_{fo}(2r_o + r_i) + \varepsilon_2 w_{fi}(r_o + 2r_i))\right] \\
&\qquad - \int_{r_i}^{r_o} m_{12} r dr - \int_{r_i}^{r_o} \nabla \bullet (\varepsilon_2 \varepsilon_{11} \rho_f V_s) r dr
\end{aligned} \quad . \qquad \text{(A.2.15)}$$

$$ADV_\theta = \frac{u_f}{r}\frac{\partial(r\varepsilon_2\rho_f v_f)}{\partial r} + \frac{v_f}{r}\frac{\partial(\varepsilon_2\rho_f v_f)}{\partial\theta} + w_f\frac{\partial(\varepsilon_2\rho_f v_f)}{\partial z} + \frac{\varepsilon_2\rho_f u_f v_f}{r} \quad . \qquad \text{(A.2.16)}$$

$$ADV_z = \frac{u_f}{r}\frac{\partial(r\varepsilon_2\rho_f w_f)}{\partial r} + \frac{v_f}{r}\frac{\partial(\varepsilon_2\rho_f w_f)}{\partial\theta} + w_f\frac{\partial(\varepsilon_2\rho_f w_f)}{\partial z} \quad . \qquad \text{(A.2.17)}$$

A.3 APPLICATION

The model for fluid pressure and velocity near the boundaries, as presented above, presumes that information from the interior calculations is available and can be used to update the boundary information.

Interior flow solution values are used for the fluid and solid velocity vectors, the fluid pressure p_f, and other quantities appearing in the functions *EXMom* [Eq. (A.2.1)], *ANGex* [Eq. (A.2.5)], *AXMex* [Eq. (A.2.8)] at r_i. This scheme also presumes that any boundary models needed for the solids are also available.

Given values from the interior solution, the pressure field on each vertical boundary is calculated from Eq. (A.2.15). Using the pressure solution, the fluid velocity gradients (shear stress) on each vertical boundary are calculated. Both the pressures and the shears are then used as boundary conditions by the interior solution scheme. The interior model for this two-way solution mode is different from the one-way

solution mode in that the near wall layer is not modeled in the interior solution. The information transferred at the top of the NW layer provides the two-way coupling where the NW layer affects the interior and vice versa. Thus, the two-way mode models the complete digester.

Depending on the solution scheme used for the interior model, it may be possible to couple the models for the boundary implicitly into the interior model so that the boundaries can be treated implicitly at each iteration of the interior solution. For the testing phase described in Sect. 4, a library routine (dgesl) for the solution to a full matrix was used.

REFERENCES

A1. J. E. Park, "Boundary Conditions For The PSL Digester Model," subcontractor report to G. E. Giles, March 16, 2001.

A2. P. He, M. Salcudean, I. Gartshore, and E. L. Bibeau, "Modeling of Kraft Two-Phase Digester Pulping Process," Digester Wall Corrosion Task Force Meeting, Seattle, WA, September, 7–8, 1999.

A3. P. He, M. Salcudean, I. Gartshore, and E. L. Bibeau, "Modeling of Kraft Two-Phase Digester Pulping Process," PowerPoint slide presentation at Digester Wall Corrosion Task Force Meeting, Seattle, WA, September 7–8, 1999.

APPENDIX B. FINITE DIFFERENCE IMPLEMENTATION OF THE NWM

The first two terms on the right-hand side (RHS) of Eq. (A.2.15) were implemented by assuming that u_f at r_o is zero and u_f at r_i is taken from the interior solution as a fixed boundary condition. Thus

$$-\left[\left(\varepsilon_2 r_o \rho_f u_f\right)\Big|_{r_o} - \left(\varepsilon_2 r_i \rho_f u_f\right)\Big|_{r_i}\right] = \varepsilon_2 r_i \rho_f u_f\Big|_{r_i}. \tag{B.1}$$

The third term of the RHS is the first term that requires a difference to replace the partials and used the following assumptions. The fluid parameters did not change with ϕ. The radius, r, is assumed to be the linear average between the inner and outer dimensions of the NW layer = $(r_o - r_i)/2$. The body force, F_f, and mass source, m_{12} are assumed zero for this stage of the development. The solid velocity is taken from the interior solution and used as a boundary condition on the NW layer model. (For test cases using nonmoving porous medium, the solid velocity is zero.)

The advection terms ADV_ϕ and ADV_z are assumed to be zero, consistent with the assumptions of the lubrication theory that the advection terms are negligible. [This assumption was tested at various times by allowing the advection terms to be calculated as shown in Eq. (A.2.16) and (A.2.17). The results of the testing showed that the advection terms had a very small effect on the results.]

Expanding the third term in the RHS of Eq. (A.2.15) and using central differences in the circumferential direction:

$$-\left(r_o - r_i\right)^3 \frac{\partial}{\partial\theta}\left[\left(\frac{\rho_f \varepsilon_2}{12\mu_f}\right)\left[ADV_\theta - \vec{n}_\theta \cdot EXMom\right]\right] = \left(r_o - r_i\right)^3 \frac{\partial}{\partial\theta}\left[\left(\frac{\rho_f \varepsilon_2}{12\mu_f}\right)\vec{n}_\theta \cdot EXMom\right] =$$

$$\left(r_o - r_i\right)^3\left(\frac{\rho_f \varepsilon_2}{12\mu_f}\right)\frac{\partial}{\partial\theta}\left[\vec{n}_\theta \cdot \alpha_{ij}\left(V_f - V_s\right)\right] = \tag{B.2}$$

$$\left(\mathrm{r\_o(k)} - \mathrm{r\_i(k)}\right)^3\left(\frac{\mathrm{rho\_f} * \mathrm{e2}}{12 * \mathrm{xmu\_f}}\right)\frac{\left[\mathrm{TEXM(j+1,k)} - \mathrm{TEXM(j-1,k)}\right]}{\left(\mathrm{th(j+1)} - \mathrm{th(j-1)}\right)}$$

where

xmu_f	= fluid viscosity,
rho_f	= fluid density,
r_o	= radius of outer limit of NWM layer,
r_i	= radius of inner limit of NWM layer,
TEXM	= value of EXMom at j,k locations,
k	= axial or z subscript,
J	= circumferential or θ subscript,
th	= circumferential coordinates.

The third line is written in the finite difference form. For three-dimensional models, the circumferential dimension is complete where the nodes at 0 radians are connected to the nodes at 2π radians in a smooth manner. No half-cells are used so that the difference equation above can be used just by changing the circumferential indices.

The fluid parameters and the solid fraction are assumed constant in the circumferential direction for the axisymmetric case tested. In three-dimensional problems, these terms must be brought into the differencing equation and evaluated at the appropriate locations. The radius values are assumed to be constant at each axial location for all terms in this development and for all models. Even in a three-

dimensional model the radius would be constant at the same axial location. The body force term of EXMom is ignored in all test cases. Of course, this whole term is zero for the axisymmetric flow case (not just for an axisymmetric model). For the more general three-dimensional case, the term TEXM in Eq. (B.2) is calculated as

$$\text{TEXM(j,k)} = \text{-ALPHAT(v\_f(l,j,k)} - \text{v\_s(l,j,k))} \,, \tag{B.3}$$

where

ALPHAT = flow resistance constant,
v_f(l,j,k) = θ component of the fluid velocity at l,j,k,
v_s(l,j,k) = θ component of the solid velocity at l,j,k.

The mass exchange between the chip and liquid, m_{12}, and the body force are assumed to be zero at this stage of the development. The velocities at the lower limit of the NWM layer are the outermost velocities from the interior flow solution or u_f, u_s, v_f, v_s, w_f, and w_s.

If the solid velocity is zero, as in the test case where a nonmoving porous medium is assumed, this becomes

$$-\left(r_o - r_i\right)^3 \left(\frac{\rho_f \varepsilon_2}{12\mu_f}\right) \frac{\partial}{\partial\theta}\left[\vec{n}_\theta \cdot \alpha_{ij} V_f\right], \tag{B.4}$$

and

$$\text{TEXM(j,k)} = -\text{Alphat} * \text{v\_f(l,j,k)} \,. \tag{B.5}$$

The flow resistance tensor, α_{ij}, is either calculated from ref. B1 or assumed to be a constant that can be adjusted to match the calculated results. In either case, the entries of the tensor are identical resulting in isotropic flow resistance. The equation supplied by ref. B1 is

$$\begin{aligned} \alpha &= 21200\frac{\varepsilon_1^2}{\varepsilon_2} + 9620000\frac{\varepsilon_1}{\varepsilon_2} V, \\ \frac{\Delta P}{\Delta L} &= \alpha \cdot V, \end{aligned} \tag{B.6}$$

where

α = flow resistance coefficient,
ε_1 = solid volume fraction,
ε_2 = liquid volume fraction,
V = fluid velocity – solid velocity (m/s),
P = pressure (Pa),
L = characteristic length (m),
Δ = change.

The fourth term of the RHS of Eq. (A.2.15) is

$$\left(\frac{r_o - r_i}{2}\right)\frac{\partial}{\partial\theta}\left[\rho_f\left(\varepsilon_2 v_{fo} + \varepsilon_2 v_{fi}\right)\right]. \tag{B.7}$$

The fluid velocity at the outer limits of the NW-model layer(which is at the wall), V_{fo}, is assumed to be zero. Thus, the finite difference form becomes

$$\frac{\left(\text{r\_o(k)} - \text{r\_i(k)}\right)}{2} * \text{rho\_f} * \frac{\left[\text{e2(i+1,k)} * \text{v\_f(j+1,k)} - \text{e2(j-1,k)v\_f(j-1,k)}\right]}{\text{(th(j+1) - th(j-1)}}. \tag{B.8}$$

If the solid fraction is assumed to be constant, then

$$\frac{\left(\text{r\_o(k)} - \text{r\_i(k)}\right)}{2} * \text{rho\_f} * \text{e2}\frac{\left[\text{v\_f(j+1,k)} - \text{v\_f(j-1,k)}\right]}{\text{(th(j+1) - th(j-1)}}. \tag{B.9}$$

Again, this whole term is zero for the axisymmetric flow cases.

The fifth term of the RHS of Eq. (A.2.15) is

$$-\left(r_o^2 - r_i^2\right)\left(r_o - r_i\right)^2\frac{\partial}{\partial z}\left[\left(\frac{\rho_f}{24\mu_f}\right)\left[ADV_z - \vec{n}_z \cdot EXMom\right]\right]. \tag{B.10}$$

As above, assuming that the advection terms are zero simplifies this term and produces a finite difference form of

$$-\left(\text{r}_\text{o}(\text{k})^2 - \text{r}_\text{i}(\text{k})^2\right)\left(\text{r}_\text{o}(\text{k}) - \text{r}_\text{i}(\text{k})\right)^2$$
$$\left[\left(\frac{-rho\_f}{48 * xmu\_f}\right)\left[\frac{\text{ZEXM(j,k+1)} - \text{ZEXM(j,k)}}{\text{DZP}}\right] + \left[\frac{\text{ZEXM(j,k)} - \text{ZEXM(j,k-1)}}{\text{DZM}}\right]\right] \tag{B.11}$$

where

ZEXM(j,k) = -ALPHAZ*(w_f(l,j,k) – w_s(l,j,k),
xmu_f = fluid viscosity,
alphaz = flow resistance constant,
w_y(l,j,k) = liquid velocity at l,j,k,
w_s(l,j,k) = solid velocity at l,j,k.

The end points and central region of the axial dimension are handled by omitting the appropriate term from the calculation. These endpoint equations are applied at the top and bottom of the digester and at the top and bottom of each exit region where the pressure is set to the data. The Poisson equation solution is not appropriate over these exits and so the pressures calculated by the interior solution code are used.

Over the central region

DZP = [z(k+1) – z(k)],
DZM = [z(k)-z(k-1)].

At the lower end point of the application of the Poisson equation solution

DZP = [z(k+1) – z(k)],
DZM = 0.0, omit the difference in the negative direction.

At the upper endpoint of the application of the Poisson equation solution

DZP = 0.0, omit the difference in the positive direction,
DZM = [z(k) – z(k-1)].

The sixth term of the RHS of Eq. (A.2.15) is

$$+\frac{(r_o - r_i)}{6}\frac{\partial}{\partial z}\left[\rho_f\left(\varepsilon_2 w_{fo}(2r_o + r_i) + \varepsilon_2 w_{fi}(r_o + 2r_i)\right)\right] . \tag{B.12}$$

The axial fluid velocity at r_o is assumed zero, which results in the finite difference form of

$$+\frac{(\text{r\_o(k)} - \text{r\_i(k)})}{12}(\text{rho\_f} * (\text{r\_o(k)} + 2\text{r\_i(k)}))$$
$$\left[\frac{(\text{e2(j,k+1)} * \text{w\_f(j,k+1)} - \text{e2(j,k)} * \text{w\_f(j,k)})}{\text{DZP}} + \frac{(\text{e2(j,k)} * \text{w\_f(j,k)} - \text{e2(j,k-1)} * \text{w\_f(j,k-1)})}{\text{DZM}}\right] . \tag{B.13}$$

The endpoints are handled in the same manner as in the fifth term above.

The last two terms of the RHS in Eq. (A.2.15) are ignored for the initial testing case using a nonmoving porous medium. Thus, there is no solid velocity and the mass source from the solid material is zero. The solid velocity terms were added into the code for comparison with the PSL data in Sect. 4.3. The mass source terms were still assumed to be zero. It is planned to add them back in as appropriate for the case being investigated.

$$-\int_{r_i}^{r_o} \dot{m}_{12} r dr - \int_{r_i}^{r_o} \nabla \bullet \left(\varepsilon_2 \varepsilon_{11} \rho_f \vec{V}_s\right) r dr . \tag{B.14}$$

The terms on the left-hand side (LHS) of Eq. A.2.15 are approximated in finite difference form to produce the coefficients of the matrix that is solved to calculate the local pressure. The first term on the LHS is

$$\frac{(r_o - r_i)}{r}\frac{\partial}{\partial \theta}\left[\left(\frac{\rho_f \varepsilon_2}{12\mu_f}\right)\frac{\partial p}{\partial \theta}\right] . \tag{B.15}$$

Which produces the following finite difference equation

$$\frac{(\text{r\_o(k)} - \text{r\_i(k)})}{(\text{r\_o(k)} + \text{r\_i(k)})/2}\left(\frac{\text{rho\_f}}{12\text{xmu\_f}}\right)\left[\frac{(\text{e2(l,j,k)p(j,k+1)} - \text{e2(l,j,k)p(j,k-1)})}{\text{DTH}^2}\right] . \quad \text{(B.16)}$$

where,

DTH = (th(j+1) – th(j-1) .

The second term on the LHS is

$$+\left(r_o^2 - r_i^2\right)\left(r_o - r_i\right)^2 \frac{\partial}{\partial z}\left[\left(\frac{\rho\varepsilon}{24\mu_f}\right)\frac{\partial p}{\partial z}\right] . \quad \text{(B.17)}$$

Which produces the following finite difference equation:

$$+(\text{r\_o(k)}^2 - \text{r\_i(k)}^2)(r\_o(k) - r\_i(k))^2\left(\frac{\text{rho\_f}}{24\text{xmu\_f}}\right)\left(\frac{2}{\delta_L + \delta_R}\right)$$
$$\left[\frac{(\text{p(l,j,k+1)e2(l,j,k+1)} - \text{p(l,j,k)e2(l,j,k)})}{\text{DZP}} + \frac{\text{p(l,j,k)e2(l,j,k)} - \text{p(l,j,k-1)e2(l,j,k-1)}}{\text{DZM}}\right] , \quad \text{(B.18)}$$

where

DZP = [z(k+1) – z(k)],
DZM = [z(k) – z(k-1)].

The terms on the LHS produce the following coefficients for the full matrix.
The main diagonal term for the node n at l,j,k:

$$\text{A(n,n)} = -2*\text{bldr3}*\text{djc}*\text{e2(l,j,k)/ddt} - 2*\text{dkc}*\text{bldsdrs}*\text{e2(l,j,k)/ddz} , \quad \text{(B.19)}$$

where

A = matrix of coefficients,
Bldr3 = bldr^3/ra,
Ra = (r(l,k) + bldr/2),
Bldr = Input (assumed) near wall layer thickness,
djc = rho_f/(12*xmu_f),
ddt = $[\text{th(j+1)-th(j)}]^2$ for j = 1,nolt-1 rows,
= $[\text{th(nolt)-th(nolt-1)}]^2$ for j = 1 row,
dkc = rho_f/(24*xmu_f),
bldsdrs = $[(\text{r(l,k)} + \text{bldr})^2 - \text{r(l,k)}^2]*\text{bldr}^2$,
ddz = [2/(DZM+DZP)][1/(DZP+DZM].

The upper and lower j diagonals are:

$$A(n, nj1) = bldr3 * djc * e2(l, j \pm 1, k)/ddt\,. \tag{B.20}$$

where

nj1 = Number of node located at l,j+1,k for the upper diagonal or
Number of node located at l,j-1,k for the lower diagonal,
ddt = (th(j) – th(j-1)) .

The upper and lower k diagonals.

$$A(n, nk1) = dkc * blrsdrs * e2(l, j, k \pm 1)/ddz\ , \tag{B.21}$$

where

ddz = (2/(DZM+DZP))(1/{DZM or DZP) [DZM is used for k– and DZP is for k+] .

REFERENCES

B1. E. L.Bibbeau, private communication to G. E. Giles, April 2, 2003.

APPENDIX C. LITERATURE SEARCH RESULTS

C.1 GENERAL DIGESTER CFD APPLICATIONS:

The most important and complete information pertinent to this project was a draft report from PSL about Digester Performance Modeling[C1] that was received in November 2000. That report reviews the prior art and helped to bring many different fields and approaches into focus. Specifically, the PSL modeling effort makes use of the Harkonen papers[C2,C3] as guides in developing a more general three-dimensional model of the complete digester for performance evaluation. Since the research tool to be developed by this ORNL project was to be used with the PSL code, in order to determine the corrosive conditions near the digester walls, the development was performed in a manner intended to be compatible with the PSL code, using common definitions and variables. Although Harkonen's work was performed in the 80's, there were no large developments or extensions of this work reported in the literature. PSL's development appeared to be unique.

C.2 SOLID-LIQUID FLOW STUDIES

It was hoped that the emerging studies of liquid-solid multiphase flow would offer insight and valuable assistance in this development. A lot of research is being performed in this area. Of particular interest are the Direct Numerical Simulations (DNS) being performed as Grand Challenge Projects.[C4-C6] The DNS studies attempt to model the physics of the liquid-solid flow on a micro-scale basis. They are extensions of the DNS simulations of turbulence phenomena and offer insights into the details of the flow. Since these studies involve a very large number of elements and can tax the available supercomputers, they are usually limited to simple geometries of small extents with a limited number of particles. Also of interest are the more limited discrete element studies.[C7-C9] The techniques available today are not capable of analyzing a complete digester with the complexities of the flow (multiple inlets/outlets, jets, and stirrers), much less including the chemical reactions of the digester. However, the information from these studies can be useful in seeing what is possible in a liquid-solid multiphase flow.

Particularly of interest are the phenomenological studies[C10] and experiments[C11] that indicate the presence of a layer near the wall that is substantially depleted in solid particles. This is generally called shear thinning or thickening. The solid particles tend to move away from areas of high shear and congregate in areas of lower shear. However, additional mechanisms must be operating since there is often a depleted zone in the center of the flow where the shear rate is lowest. The mechanism of moving away from the wall is driven by pressure gradients. If the particle size is smaller than the boundary layer thickness, there can develop a differential pressure on the particle that will tend to force it away from the wall until it is outside of the boundary layer. If the particle is larger than the boundary layer thickness, then another process can produce a force to move the particle away from the wall.[C.5] This process is similar to that of an airplane wing near the ground (in ground effect = less than one wing span). This ground effect enhances the lift of the wing (particle) due to the presence of the ground plane. Enhanced lift is more evident on nonspherical particles. These particles will respond to this force and tend to move away from the wall. This ground effect is only active near the wall (approximately a chip diameter), and thus the chips will move only a short distance from the wall. The nonspherical particle orientation is required to be more or less parallel to the wall for this effect to be significant. Fortunately, the shearing force will tend to orient a particle parallel to the wall.[C12] Even in collections with more than one particle, they tend to orient parallel to the wall.[C13] Although there is a tendency for nonspherical particles to orient parallel to walls, high solid fraction solutions could prevent this orienting force from accomplishing a complete alignment.

Depletion of the solid particles near the wall could provide a relatively clear layer that might allow more rapid transport of chemical species down the wall than in the interior flow. Substantial

modifications to the fluid in this area could make the processes at the wall much different from those in the interior. The details of the shear thinning depend greatly on the nature of the liquid and can actually reverse these trends for a visco-elastic fluid (such as concentrated suspensions).[C14]

During inspections of the digesters, there is sometimes a pattern evident in the corrosion pits. Spiral streaks of pits sometimes are seen. The mechanism that forms these streaks is not known. It may be due to a flow condition that causes a local chemical concentration that follows the fluid flow path. An alternative explanation may be due to the flow dragging the wood chips along in similar paths. The chips may actually rub along the wall. If the flow pattern is repeatable, then this might explain the pit pattern. This later mechanism is called erosion-corrosion. The process is well known in pipeline type flows and several investigations have been reported. However, most of the study has been done for hard particles in relatively dilute concentrations.[C15,C16] Although locally enhanced corrosion is found in these studies, they generally require some flow upset that causes the particles to impact the surface reducing the oxide layer thickness which can allow electrochemical corrosion to proceed faster than in other locations. It seems unlikely that impacting wood chips (saturated with liquor) could destroy the protective oxide layer in a digester. A more likely scenario would be for the wood chips to rub along the wall, incrementally reducing the oxide layer. Streaks of pits might indicate a flow system that causes wood chips to follow similar paths along the wall. However, no references were found that considered the frictional destruction of the oxide layer. The existence of erosion-corrosion seems incompatible with the existence of a clear layer discussed above.

REFERENCES

C1. P. He, M. Salcudean, I. Gartshore, and E. L. Bibeau, “Modeling of Kraft Two-Phase Digester Pulping Process,” Digester Wall Corrosion Task Force Meeting, Seattle, WA, September 1999.

C2. E. J. Harkonen, “A Mathematical Model For Two-Phase Flow In A Continuous Digester,” *TAPPI J.*, 70, no. 12, pp.122–126, December 1987.

C3. E. J. Harkonen, “A Mathematical Model For Two-Phase Flow,” Acta Polytechnica Scandinavica, Mechanical, Eng. Ser 88, Helsinki, 1984.

C4. D. D. Joseph, D. Ocnado, P. Y. Huang, “Slip Velocity and Lift,” *J. of Fluid Mechanics*, 2003.

C5. N. A. Patankar, P. Y. Huang, T. Ko, D. D. Joseph, “Lift-Off Of A Single Particle In Newtonian And Viscoelastic Fluid By Direct Numerical Simulation,” *J. of Fluid Mechanics*, 38, pp. 67–100.

C6. D. W. I. Rouson, J. K Eaton, “On The Preferential Concentration Of Solid Particles In Turbulent Channel Flow,” *J. Fluid Mechanics*, 428, pp. 149–169, 2001.

C7. H. G. Choi, D. D. Joseph, “Fluidization By Lift Of 300 Circular Particles In Plane Poiseuille Flow By Direct Numerical Simulation,” *J. Fluid Mechanics*, 438, pp. 101–128, 2001.

C8. M. L. Hunt, “Discrete Element Simulations for Granular Flows: Effective Thermal Conductivity and Self-Diffusivity,” *International J. Heat Mass Transfer*, 40, pp. 3059-3068, 1997.

C9. R. Kedia, M.L. Hunt, and T. Colonius, “Numerical Simulations of Heat Transfer in Taylor-Couette Flow,” *J. Heat Transfer*, 120, pp. 65-71, 1998.

C10. J. F. Brady, “Modeling Suspension Flows,” FED-Vol 189, Liquid-Solid Flows, ASME, 1994.

C11. A. Shauly, A. Averbakh, A. Nir, R. Semiat, “Slow Viscous Flows Of Highly Concentrated Suspensions – Part II: Particle Migration, Velocity And Concentration Profiles In Rectangular Ducts,” *Int. J. Multiphase Flow*, 23, no. 4, pp. 613–629, 1997.

C12. K. M. Burget, G. A. Suresh, “An Experimental Investigation Of Fiber Motion Near Solid Boundaries In Simple Shear Flow,” FED-Vol 189, p. 59, Liquid-Solid Flows, ASME, 1994,

C13. D. Qi, “Simulations Of Fluidization Of Cylindrical Multi-Particles In A Three-Dimensional Space,*” Int. J. of Multiphase Flow*, 27, pp.107–118, 2001.

C14. P. Singh, D. D. Joseph, T. I. Hesla, R. Glowinski, T. W. Pan, “A Distributed Lagrange Multiplier/Fictitious Domain Method For Viscoelastic Particulate Flows,” *J. Non-Newtonian Fluid Mech.,* 91, pp. 165–188, 2000

C15. S. Nesic, J. Postlethwaite, D. Bergstrom, “Modelling Erosion-Corrosion in Disturbed Liquid-Solid Flow,” FED-Vol 189, p. 71, Liquid-Solid Flows, ASME, 1994,
C16. Z. Zhang, X. Cheng, Y. Zheng, et. al, “Numerical Simulation Of Erosion-Corrosion In Liquid-Solid Two Phase Flow,” *Chinese J. of Chem. Eng.,* 8, no. 4, pp. 347–355, 2000.

APPENDIX D. CLEAR LAYER INVESTIGATION

In the liquid-solid flow literature, there is evidence of the existence of a layer substantially depleted of solid particles near the wall. In order to determine the possible effect of such a clear layer, a set of models, using the simplified digester discussed in Sect. 4.1, were modified to allow a layer of fluid to flow free in a gap between the nonmoving, porous medium and the wall. The clear layers investigated ranged from 1mm up to 5 cm. From the literature, a 5-mm-clear layer is the most likely thickness for a range of flows. The same boundary conditions were applied to the clear layer model as discussed in Sect. 4.1. The clear layer does not seem to affect the bulk flow greatly. The fluid velocities in the porous medium, flow patterns, and pressure distribution in the bulk, are very similar to the model where the porous medium extends to the wall.

The fluid flow vectors for a 5 mm clear model are shown in Fig. D.1. This figure is a detail plot of the region immediately above the ES exit, where the axial flow is the highest. Included in this figure are the flow vectors, streamlines, and fringe patterns showing the fluid speed. The relative difference between the flow in the clear layer and in the bulk flow can be readily seen.

Figure D.2 compares the axial flow velocity of two cases with differing clear layer thicknesses (1 and 5 mm). The axial velocity curves for the bulk flow are very similar to the completely porous models discussed in Sect. 4.1. This is because of the relatively small volume that the clear layer comprises. The mass flow in the clear layer is not very large, even if the velocities are much larger, and thus the total flow down the digester is not greatly affected by the clear layer.

The 5-mm case showed a much greater difference between the velocity in the bulk and that in the clear layer than was present in the 1-mm case. This greatly enhanced velocity would allow for the more rapid transport of fluid and chemical species along the wall than in the bulk flow. This condition might explain some puzzling experimental data found in the Kamloops digester.[D1] In this experiment, the electrochemical noise instrument was shown to be reacting to a change in feed composition much more rapidly than bulk flow movement could explain. The enhanced velocity of such a clear layer in the calculations could support this finding. An estimate of the time to transit from the top down to the level of the top of the ES exit can be made. For the 5 mm clear layer, the bulk flow is estimated to take 76 s to transit down to the top of the ES exit, while the clear layer transit time is estimated to be 2.3 s. In a mode that more accurately reflects a real digester design, these time differences could be much larger. The simplified model shows that there can be an order of magnitude difference in the transit times along the clear layer as compared to the interior flow. Recirculations and other complex flow patterns could alter this comparison by delaying the interior flow even more. Of course, step changes in the radius would temporarily (or permanently) disrupt the clear layer.

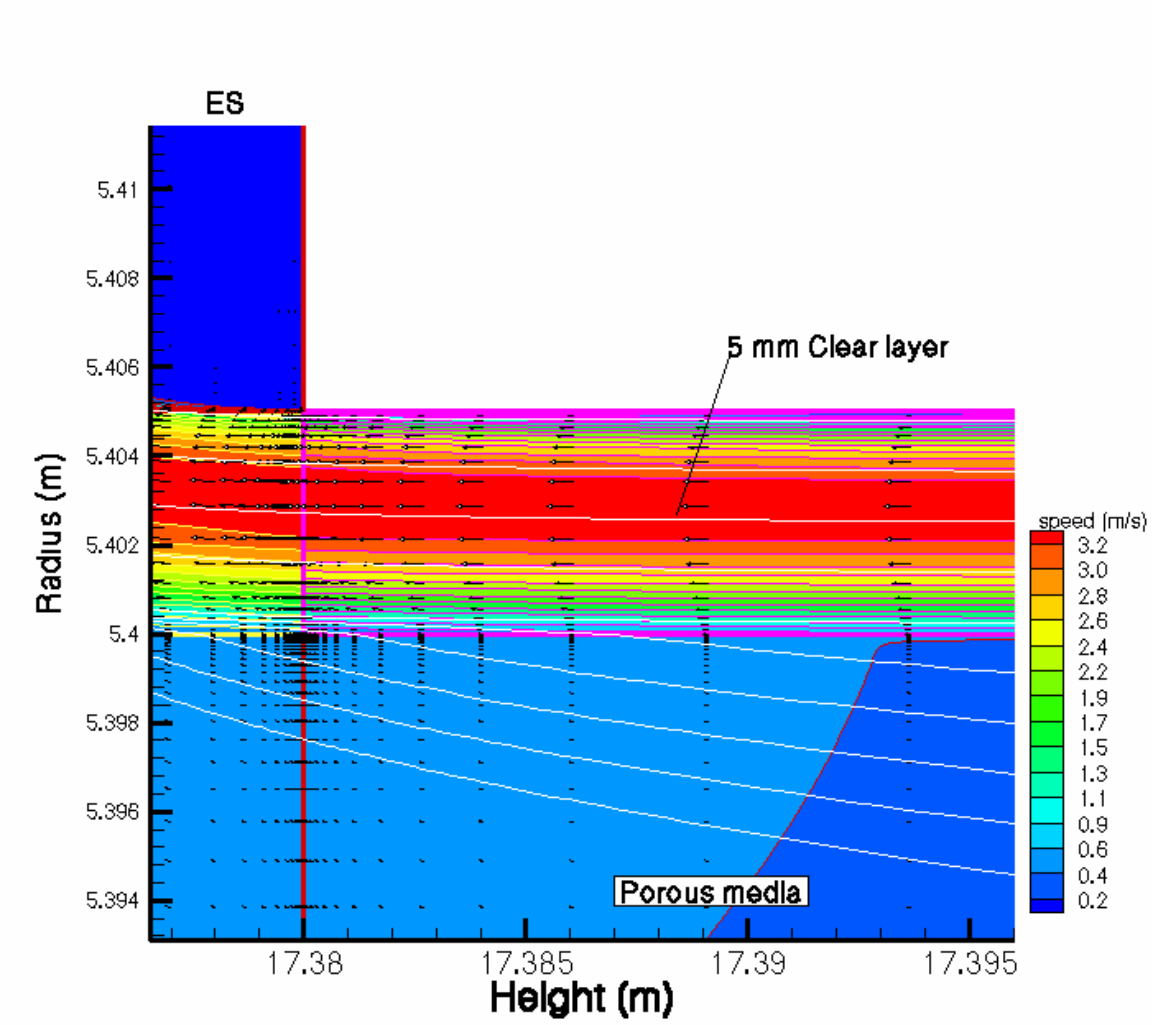

Fig. D.1. Flow vectors, speed contour, and streamlines are shown for a 5-mm-clear model for a region immediately above the ES exit.

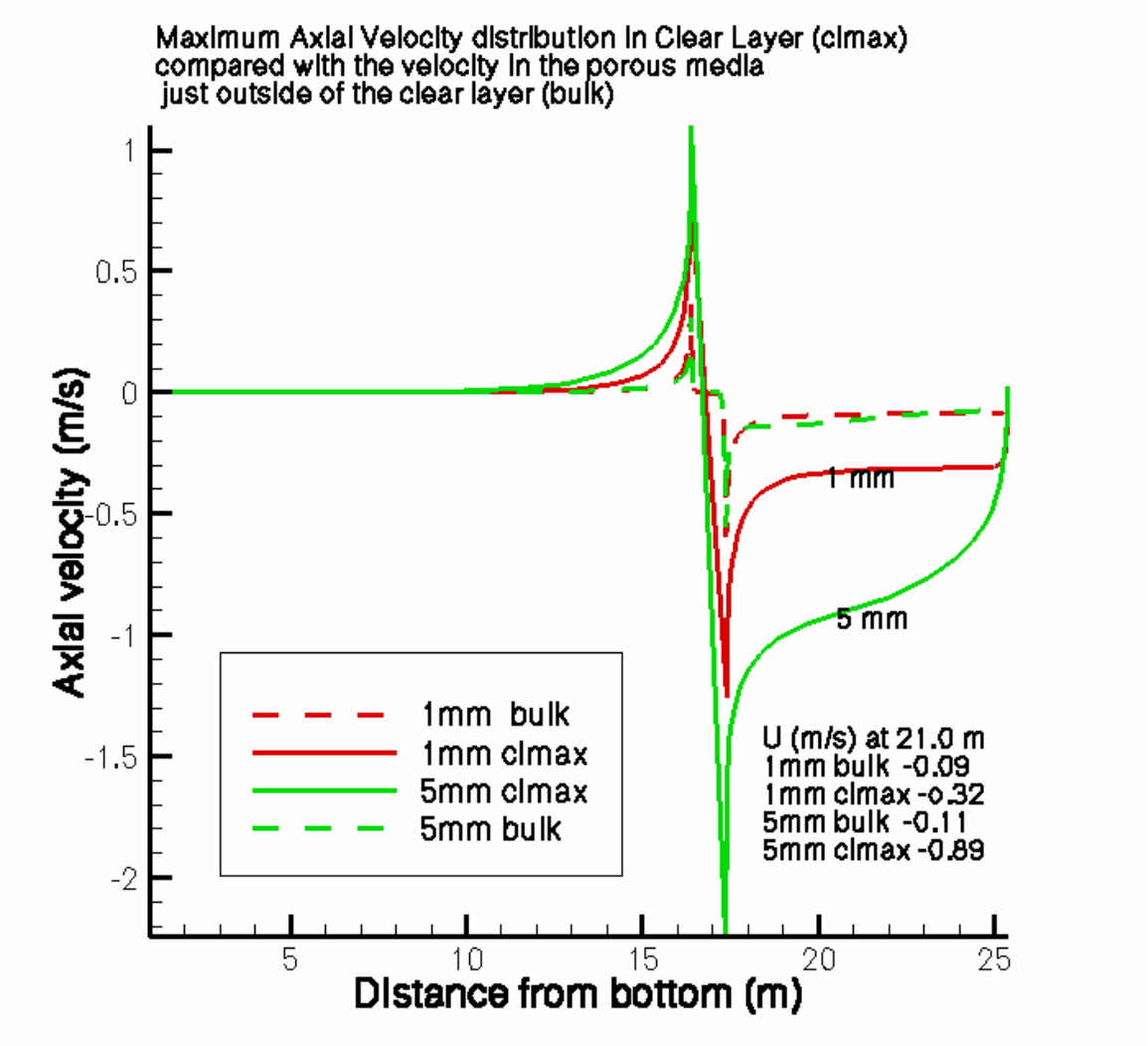

Fig. D.2. Comparison of the axial flow velocity distribution along the wall for two clear layer cases [in bulk flow(dashed) and in clear layer(solid)].

REFERENCES

D1. S. J. Pawel, D. W. Townley, M. E. Gorog, D. F. Wilson, "Correlation of the Process Data and Electrochemical Noise to Assess Kraft Digester Corrosion: Kamloops Experiment," ORNL/TM/2002/33, April 2002.

APPENDIX E. OPTIMIZING TERMS TO FIND DEVELOPMENT ERRORS

In debugging the NWM code, a technique was developed to determine which term of the equations might have an error. A weighting function on each term in the equations was applied and the weights were varied until a best match (in the RMS sense) was found. This procedure becomes an n-dimensional nonlinear search process (n is either 4 or 8 depending on the test case used). The search used a simple technique in which the minimum RMS is found for a weight function and then the process is repeated for each weight function in turn. This loop is repeated many times while the best weight functions from the previous iterations are used. This simple-minded search technique can require many iterations before the change in the RMS value is within a selected value. Usually, but not always, a change of the RMS value over an iteration of 1×10^{-6} produces a fairly good match (RMS values less than 1×10^{-2}) with the target (CFX4) profile. This technique was useful in the debugging process for identifying some coding and development errors. Isolating the potential error by terms was useful in that it concentrated the search on a more limited portion of the equations. As an example, Fig. E.1 shows the results of applying this optimization technique in an intermediate version of the NWM code to the model in Sect. 4.3. The non-optimized results are quite different from the PSL results indicating a potential problem. The weights that produced the excellent match in the figure were 0.5 for the sixth term and -1.5708 (approximately $\pi/2$) for the eighth term. This problem was not sensitive to the second and fifth terms. (The change in these weights for the last iteration was less than 1×10^{-6}.) These values indicated errors in the implementation or development. Using this process, sign errors, incorrect exponents, or incorrect formulations were identified.

Furthermore, if these weights for several different cases (differing inlet flows, mesh size or mesh non-uniformity) converge to the same (or nearly the same) values, this would indicate a systemic error in a specific term. If the trend in optimized weights as a function of independent variable (flow rate or local mesh size) matches the change in independent variable, then that would indicate which variable might have been mishandled in the development or implementation.

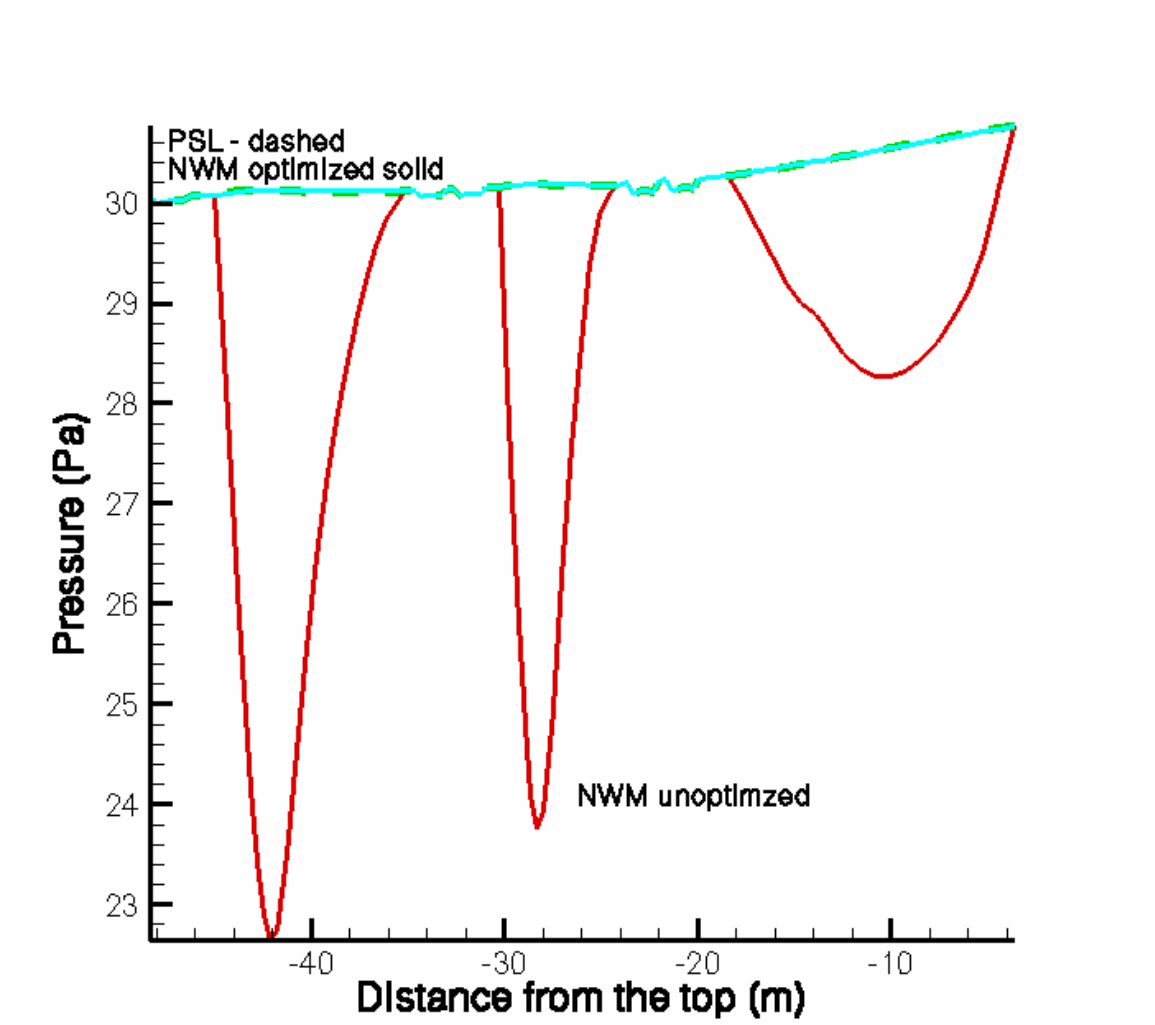

Fig. E.1. Pressure distribution for optimized NWM compared with PSL results and non-optimized NWM results.

INTERNAL DISTRIBUTION

1−5. G. E. Giles
6. D. M. Hetrick
7−11. S. J. Pawel
12. B. A. Worley
13. D. F. Wilson
14. Central Research Library
15. ORNL Laboratory Records − RC
16. ORNL Laboratory Records – OSTI

EXTERNAL DISTRIBUTION

17. D. C. Crowe, International Paper, Mfg. Tech. Center, 6285 Tri-Ridge Blvd., P.O. Box 7910, Loveland, OH 45140
18. M. E. Gorog, WTC1B40, Weyerhaeuser, P.O. Box 9777, Federal Way, WA 98063-9777
19. D. E. Roy, Glatfelter Company, 228 South Main St., Spring Grove, PA 17362
20. M. Salcudean, 1938 Western Parkway, Vancouver, V6T 1V5, British Columbia, Canada
21. W. B. A. Sharp, MeadWestvaco, Laurel Technical Center, 11101 Johns Hopkins Rd., Laurel, MD 20723-6006
22. P. M. Singh, Institute of Paper Science and Technology, 500 10th Street, Atlanta, GA 30318-5794
23. D. W. Townley, M. J. Schiff and Associates, 431 W. Baseline Rd., Claremont, CA 91911